NACA RM L56F14

RESEARCH MEMORANDUM

EXPERIMENTAL INVESTIGATION OF A TRANSONIC AXIAL-FLOW-COMPRESSOR ROTOR DESIGNED FOR SONIC INLET VELOCITY WITH AN INLET HUB-TIP RADIUS RATIO OF 0.35

By Emanuel Boxer and Peter T. Bernot

Langley Aeronautical Laboratory
Langley Field, Va.

NATIONAL ADVISORY COMMITTEE
FOR AERONAUTICS

WASHINGTON
September 28, 1956
Declassified January 12, 1961

NATIONAL ADVISORY COMMITTEE FOR AERONAUTICS

RESEARCH MEMORANDUM

EXPERIMENTAL INVESTIGATION OF A TRANSONIC AXIAL-FLOW-COMPRESSOR ROTOR DESIGNED FOR SONIC INLET VELOCITY WITH AN INLET HUB-TIP RADIUS RATIO OF 0.35

By Emanuel Boxer and Peter T. Bernot

SUMMARY

A high-flow sonic-inlet compressor rotor employing double-circular-arc blade sections was designed and tested in Freon-12. At an equivalent tip speed of 1,000 feet per second in air, the rotor was designed for a specific weight flow of air of 43.2 lb/sec/ft^2 of frontal area with an inlet hub-tip ratio of 0.35 and a pressure ratio of 1.40 at an efficiency of 90 percent.

Test results at design speed yielded a specific weight flow of air of 41.3 lb/sec/ft^2 with a pressure ratio of 1.38 at a peak efficiency of 80 percent. Maximum specific weight flow of 42.13 lb/sec/ft^2 was obtained at 110 percent of design speed at a peak efficiency of 75 percent while a maximum efficiency of 85 percent was reached at 60 and 90 percent of design speed.

Sonic inlet conditions were not attained because of the supersonic wave pattern generated by the curved entrance region on the convex surface of the blades which restricted the axial Mach number to a value of 0.81.

Comparison of results with those of a rotor similar in camber and solidity indicates that for efficient operation the thickness-chord ratio and blade setting angle over the range presented are of secondary importance to the relative inlet Mach number level.

INTRODUCTION

One of the advantages in the use of a transonic compressor for turbojet engines is its ability to accommodate a greater weight flow of air than more conventionally designed compressors, which in turn permits an increase in engine thrust per unit frontal area in direct proportion to

the increased air-flow capacity. It has been shown (ref. 1) that it is possible to compress efficiently 37 lb/sec/ft^2 in a rotor with a hub-tip radius ratio of 0.35 at a tip speed of 972 feet per second and an inlet axial Mach number of 0.63. In order to further increase the air flow, it is necessary either to decrease the hub-tip radius ratio or to increase the axial inlet Mach number or both. The hub-tip radius ratio of 0.35 is felt to represent a practical lower limit due to structural and constructional difficulties, but were it possible to reduce the inlet inner radius to zero, the flow capacity would increase 12 percent, whereas raising the inlet axial Mach number from approximately 0.6 to 1.0 would increase the air flow 18 percent. The desirability of maintaining as high a pressure ratio per stage as possible requires a high rotor tip speed. Thus, designing for higher inflow (axial) velocities will result in rotor relative inlet Mach numbers considerably in excess of 1.10, the limiting value for which good efficiencies were obtained (refs. 1 to 4).

For flight at moderate supersonic speeds (Mach numbers on the order of 1.5 to 1.8) a decrease in compressor efficiency due to the higher relative inlet Mach number may be partially compensated by improved inlet diffuser pressure recovery. In this range of flight speeds, a major source of diffuser loss can be attributed to the viscous behavior of the boundary layer rather than to shock losses. Reducing the diffusion required upstream of the compressor should reduce the pressure losses somewhat so that the overall efficiency of compression from free-stream conditions will not decrease in proportion to a decrease in compressor efficiency. (See ref. 5.)

In order to explore the operation of a transonic rotor at a high inlet axial Mach number, a 12-inch-diameter rotor with a hub-tip radius ratio of 0.35 designed for a tip speed of 1,000 feet per second, an inlet axial Mach number of 1.0, a total pressure ratio of 1.40, and a specific weight flow of 43.2 lb/sec/ft^2 was built and tested using Freon-12 gas as the testing medium. Thin double-circular-arc sections were selected because previous results (refs. 2 and 3) indicated efficient performance at transonic inlet relative Mach numbers and reasonable agreement with low-speed deviation angle predictions. Tests were made through a speed range of 60 to 110 percent of the design value.

SYMBOLS

A_f frontal area, sq ft

c blade chord, in.

c_p specific heat at constant pressure, $\frac{\text{ft-lb}}{(\text{slugs})(^\circ\text{F})}$

D	diffusion factor, $1 - \frac{V_{2R}}{V_{1R}} + \frac{\Delta V_T}{2\sigma V_{1R}}$
$\frac{U_t}{\sqrt{\theta}}$	equivalent tip speed, ft/sec
F_c	compressibility factor
G	blade gap, in.
g	acceleration due to gravity, 32.17 ft/sec^2
i	angle of incidence, angle between inlet-air direction and tangent to blade mean camber line at leading edge, deg
r_{le}	leading-edge radius, in.
M	Mach number
n	rotor speed, rps
P	total pressure, lb/sq ft
p	static pressure, lb/sq ft
$\frac{\Delta p}{qF_c}$	diffusion coefficient, $\frac{p_2 - p_1}{P_{1R} - p_1}$
Q	torque, ft-lb
q	dynamic pressure, lb/sq ft
r	radius, ft
T	stagnation temperature, $^{\circ}R$
t	blade thickness, in.
U	blade velocity, $2\pi nr$, ft/sec
V	flow velocity, ft/sec
W	weight flow, lb/sec
β	angle between velocity vector and rotor axis, deg
γ	ratio of specific heats

Δ deviation angle, angle between tangent to mean camber line at blade trailing edge and relative air direction leaving blade, deg

ΔV_T change in tangential velocity across rotor, ft/sec

δ ratio of inlet total pressure to standard NACA sea-level pressure, 2,116 lb/sq ft

ζ blade-setting angle, $\beta_{1R} - i - \frac{\phi}{2}$, deg

η_{ad} efficiency based upon temperature measurement

η_M efficiency based upon momentum change

η_Q efficiency based upon torque measurement

θ ratio of inlet total temperature to standard NACA sea-level temperature, 518.6° R

ρ flow density, lb/cu ft

σ solidity, ratio of chord to gap

ϕ blade camber angle, deg

ω total pressure loss parameter, $\frac{P_{1R} - P_{2R}}{P_{1R} - p_1}$

Subscripts:

a axial

h hub

m mean

o settling chamber

p pressure surface

R relative to rotor

s suction surface

T tangential

t tip

V venturi

1 upstream of rotor

2 downstream of rotor

Superscripts:

Bar over parameter indicates mass-weighted average.

GENERAL AERODYNAMIC DESIGN

Rotor Design

In order to explore the high-subsonic-inflow regime of a high-flow transonic compressor, a 12-inch-diameter rotor with an inlet hub-tip radius ratio of 0.35 was designed for the following prescribed conditions:

(1) An equivalent tip speed of 1,000 ft/sec
(2) Sonic axial inlet velocity
(3) No inlet guide vanes
(4) A 5-percent reduction in the annular area through the rotor
(5) A linear tangential velocity distribution downstream of the rotor given by the equation $V_T = 862 - 923r$
(6) A polytropic efficiency of 0.90 at all radial stations

The downstream exit conditions were calculated by the method given in reference 6 assuming simple radial equilibrium and constant entropy with no area allowance for the boundary-layer displacement thickness. The resulting flow parameters are tabulated in figure 1.

The diffusion factor D, calculated for the required velocity diagrams and selected solidities, is a maximum at the midthird of the blade span. (See fig. 1.) Although the D factor at the tip is in the rising loss coefficient region of the correlation curve presented in reference 7, efficiencies of 90 percent were previously obtained for this condition, albeit at lower Mach numbers. At the mean and hub radii, the measured loss coefficients shown in reference 7 were independent of diffusion factor D for the required range. Based on previous experience at lower relative Mach numbers, the rotor design requirements, while definitely not conservative, were within the limits prescribed for reasonably high efficiency. In order to estimate the effect of Mach number, the diffusion coefficient $\Delta p/qF_c$ near the tip was compared with that obtained by a

supersonic compressor at a relative inlet Mach number of 1.35 and found to be of equal magnitude. At this condition the section efficiency was 80 percent. The compressor in question was reported in reference 8; however, the data at lower than design speeds were unpublished.

The foregoing considerations led to a rotor designed to produce an average total pressure ratio of 1.40 with a weight flow of air of 43.2 lb/sec/sq ft of frontal area.

Blade Design

Circular-arc blade sections were selected for incorporation in the test rotor because transonic test data were not available on NACA 65-series blower blade sections at the time the rotor was designed. The circular-arc blade sections were formed as shown in figure 2. Because the thickness-chord ratio is low, varying from 0.05 at the hub to 0.035 at the tip, the mean line is essentially a circular arc. The blade camber angles, therefore, were selected by means of Carter's rule for circular-arc mean lines (ref. 9) with the following modifications: (a) An angle of incidence i of 2° was assumed for all radial stations and was based upon results of high-speed cascade tests presented in reference 10, and (b) the deviation angles were increased by 2° since previous transonic rotor results of similar sections (ref. 3) indicated an underturning of approximately 2°.

The tip solidity of 0.8 was chosen to provide sufficient blade overlap to stabilize a strong shock in the blade passage which, from two-dimensional considerations, is necessary to provide the required static-pressure rise. Twelve blades were selected for the rotor with a constant chord of 2.51 inches. As a result, the solidity at $r/r_t = 0.40$ is 2.0.

An examination of the blade sections revealed that the two-dimensional-flow area within the blade passage was greater than the design relative inflow area for all but the hub section. The area at the trailing edge of the hub section was approximately 5 percent less than that at the inlet. However, the three-dimensional-flow area between blades increases rather uniformly from leading edge to trailing edge in such a way that the overall exit area is about 9.3 percent greater than the inlet area.

Rotor Construction

The rotor hub and blades were integrally formed of fiber glass, polyester resin, and balsa wood. The diametrically opposed blades were molded on opposite ends of prestressed fiber glass strands which were first woven through a balsa-wood hub. In this manner, the centrifugal

blade loads are resisted in the most efficient manner. A three-quarter rear view of the test rotor appears in figure 3. Additional information concerning the technique of plastic rotor construction is given in reference 1.

APPARATUS AND METHODS

Test Facility

A schematic diagram of the compressor test stand is presented in figure 4. The test rotor was driven through a 4 to 1 speed increaser by a 3,000-horsepower induction motor powered by a variable-frequency electrical power source. The closed-loop test stand was originally designed for use with 16-inch-diameter supersonic compressors of high radius ratio (ref. 8). In order to permit the testing of a high-flow single-stage transonic compressor, it was necessary to reduce the rotor tip diameter to 12 inches and so prevent choking of the flow in the radial diffuser. In addition, both 60-mesh screens located ahead of the venturi meter were removed to eliminate the principal disposable source of pressure loss in the system. It was found by previous tests that the absence of these screens did not affect the weight flow measurement. A detail drawing of the test section is presented in figure 5. The survey stations as shown are about $1\frac{3}{4}$ inches ahead and behind the rotor.

Instrumentation and Data Reduction

The instrumentation and computational procedures are similar to those described in reference 1. The inlet pressures were measured by four static orifices equally spaced around the circumference located near the upstream survey station on both inner and outer walls and by static orifices in the settling chamber. Four shielded iron-constantan thermocouples mounted in the settling chamber measured the inlet stagnation temperatures directly by means of a commercial self-balancing-type temperature indicator. The inlet flow conditions were calculated assuming a linear variation of static pressure across the passage. Results of preliminary upstream surveys at four circumferential positions indicated that an average swirl of 1.1° in the direction of rotation was present and its effect was included in the performance calculations.

The static and total pressures as well as flow angle were measured at 10 radial positions at the downstream survey position by means of a calibrated prism-type survey probe shown in figure 6. Four static-pressure orifices on both inner and outer walls, equally spaced circumferentially, were located at the downstream survey station. The radial distribution

of static pressure was obtained from a curve faired through the wall tap and survey probe measured values. The total-pressure readings were corrected for normal shock losses when the absolute exiting Mach number was greater than 1.0. All pressure measurements were made by photographing a multitube common-well mercury manometer.

The stagnation temperature rise across the rotor was measured by three calibrated chromel-alumel thermocouple rakes. Each rake, one of which is shown in figure 7, was composed of four doubly shielded thermocouples. Two of the rakes spaced 90° apart were located downstream of the rotor and were radially positioned to cover the passage. The third rake was centrally located in the passage upstream of the rotor. The difference in potential between the upstream and downstream thermocouples was measured by means of a d-c preamplifier and recording potentiometer.

Although the weight flow entering and leaving the rotor was determined by integration of the elemental flow parameter ρV_a, the overall weight flow presented herein was measured by means of the calibrated venturi meter. The rotor tip speed was measured by means of a commercial stroboscopic tuning-fork-controlled instrument in conjunction with the output frequency of an alternator mounted on the drive-motor shaft.

In order to compute the blade-element parameters such as loss coefficient, D factor, and efficiency, which are dependent upon flow conditions on a given streamline across the rotor, it was assumed that streamlines exist between centers of equal annular area at each survey station. The section efficiency was computed by two methods: one in which η_{ad} was based upon measured temperature rise; and the other, η_M based upon the momentum change across the rotor where:

$$\eta_{ad} = \frac{\left(\frac{P_2}{P_1}\right)^{\frac{\gamma-1}{\gamma}} - 1}{\frac{T_2}{T_1} - 1}$$

and

$$\eta_M = \frac{c_p T_1 \left[\left(\frac{P_2}{P_1}\right)^{\frac{\gamma-1}{\gamma}} - 1\right]}{U_2 V_{T_2} - U_1 V_{T_1}}$$

The rotor overall performance parameters $\bar{\eta}_{ad}$, $\bar{\eta}_M$, and $\bar{P}_2/P_1$ were obtained by mass weighting the measured elemental values. In addition, a

rotor efficiency $\bar{\eta}_Q$ based upon input torque measurements obtained by a strain-gage torquemeter was determined by use of the following equation:

$$\bar{\eta}_Q = \frac{c_p T_1 \int_{r_h^2}^{r_t^2} \left[\left(\frac{P_2}{P_1}\right)^{\frac{\gamma-1}{\gamma}} - 1\right] \rho_1 V a_1 d\left(r^2\right)}{2ngQ}$$

Test Procedure

Tests were made through a speed range of 60 to 110 percent of design speed using Freon-12 gas as the test medium. The inlet stagnation pressure was maintained at about 20 inches of mercury absolute by means of an automatic inbleed control valve in the recirculating Freon supply system. The air leakage was such that during operation the Freon purity in the test stand was never less than 96 percent by volume.

At a given speed the ranges of weight flow and pressure ratio were observed as the throttle was varied from full open to that at which surge occurred. Data were then taken at four or five fixed throttle settings to cover the entire operating range. Torque meter readings were recorded at the same time the manometer was photographed to avoid errors due to any settling chamber pressure variation as the survey was made. The inlet stagnation temperature was permitted to reach an equilibrium value with full cooling water flow to the radiators before the temperatures were recorded.

Precision of Data

Due to the nonuniform nature of the flow downstream of the rotor, it is difficult to ascertain the accuracy of each pressure, temperature, and angle measurement on a quantitative basis. Evaluation of radial flow and circumferential flow variation was not made in these tests. However, the accuracy of the data is indicated by the agreement of the weight flows measured at the two stations as shown in figure 8. Excluding the values obtained for 60 percent of design tip speed, the inlet weight flow was within 1.5 percent while the outlet flow was within 4 percent of that measured by the venturi meter. Noisy operation at the lowest tip speed may explain the larger divergence of weight flow measurements since the rotor may have been operating in a partially stalled condition.

The reasonable agreement as obtained for the overall results (especially the weight-flow measurements at the rotor inlet) tends to indicate a good degree of reliability of the pressure and temperature measurements. The blade-element results therefore are believed to be valid.

A tabulation of the accuracies of the various data measurements is presented as follows:

Tip speed, percent	0.05
Outlet flow angle, deg	0.5
Venturi weight flow, percent	1.0
Rotor temperature rise, percent	1.0
Torque input, percent	0.5
Pressure, in. Hg	0.030
Rotor inlet and venturi temperatures, $^{\circ}F$	1.0

RESULTS AND DISCUSSION

It is usual to express the performance of a compressor in terms of the quantity of air handled for a given angular velocity or tip speed. For direct comparison with the numerical values familiar to compressor designers, these results as obtained in Freon-12 gas have been converted to the equivalent values in air by the method presented in reference 11.

Overall performance.- The overall performance of the rotor is presented in figure 9. At an equivalent design tip speed of 1,000 feet per second, a peak pressure ratio and efficiency of 1.38 and 80 percent, respectively, were obtained at a specific weight flow of 41.3 lb/sec/sq ft. At 110 percent of design speed, the corresponding values were 1.45, 75 percent, and 41.8 lb/sec/sq ft. A maximum efficiency of 85 percent was obtained at 60 and 90 percent of design speed.

An examination of the performance characteristics will reveal certain modes of operation peculiar to the test facility and rotor and not noted in previously reported results of transonic rotors. At equivalent tip speeds up to and including 900 feet per second, the high-flow end of the characteristic curve is missing and at design speeds and above the weight flow range is extremely small. The failure to obtain the high-flow end of the low-speed characteristic curves is due to the high loop losses associated with the high design rate of flow and the low pressure rise produced by the rotor. At 60 percent of design speed, the positive slope of the efficiency curve and the flat pressure characteristic are indicative of operation with rotating or tip stall. This was borne out by unsteady pressure indication on the manometer as well as by the difficulty of determining the actual surge point by audible means.

The small weight-flow range exhibited at design speed was anticipated for this rotor because of the high design inlet axial Mach number. At Mach numbers near 1.0, significant variations in Mach number produce small variations in mass flow per unit area. For example, the test rotor induced a mass flow of 97 percent of the design value, yet the axial inlet Mach number was 20 percent below the design value.

At an equivalent tip speed of 1,100 feet per second, the maximum rate of flow is essentially identical to that obtained at design speed. Because the pressure characteristic curve is very nearly vertical and the peak efficiency occurs at peak pressure ratio, which together are indicative of operation similar to that of shock-in-rotor supersonic compressors, the explanation for the behavior of the maximum weight-flow—speed relationship for this rotor may be obtained from two-dimensional supersonic compressor theory of reference 12. For a rotor blade section operating at supersonic relative velocities, the minimum flow inlet angle is determined by the wave pattern upstream of the rotor and is not necessarily dependent upon choking within the passage formed by the blades or the degree to which the back pressure is lowered as is the case for subsonic relative inlet velocities. The upstream wave pattern is in turn a function of the rotational speed, solidity, and the geometry of the blade leading edge and "entrance region." In reference 12 the entrance region is defined as that forward portion of the suction surface from which Mach waves originating on the surface will "escape" ahead of the following blade. For steady flow, the upstream wave pattern must be composed of compression and expansion waves of equal total strength. Because the expansion waves generated on a convex-circular-arc entrance region partially cancel the compression waves on the following blade as well as those produced by the same blade, the upstream undisturbed relative inlet Mach number must be equal in magnitude and direction to that of some point on the entrance region (see ref. 13 for more detail). As the rotational speed is increased, the length of the entrance region is shortened and the total pressure loss across a detached bow shock is increased. These combined effects will tend to increase the minimum flow inlet angle.

For the subject rotor, which, incidentally, is operating with the highest inlet axial Mach number of any transonic or supersonic compressor yet reported, the net effect of an increase of rotor tip speed from 1,000 to 1,100 feet per second upon the measured average inlet axial Mach number was an increase from 0.813 to 0.820.

Radial distribution.- The radial distribution of several rotor performance parameters is presented in figures 10 to 16 for 60, 90, 100, and 110 percent of design speed. These results are shown on plots wherein the ordinate scale is displaced an incremental amount for each curve which minimizes crowding and aids in interpreting more easily the relative variations of the curves on a given plot. Figure 17 shows the radial distribution of absolute flow angle leaving the rotor at design speed.

The tip relative inlet Mach number for these tests varied from 0.61 to 1.34 as can be seen in figure 10. At design speed, the maximum relative Mach number at the hub and tip were 0.85 and 1.25, respectively, with only slight changes due to throttling. Because the design tip value of 1.4 was not attained, a lower-than-design inlet axial Mach number is indicated. Rather than achieving sonic axial inlet velocity as designed, the measured axial Mach number was about 0.81.

The radial variation of the relative Mach number leaving the rotor is presented in figure 11. In general, it is seen to be almost uniform across the passage except for the region of rapid fall-off from about 0.45 foot to the tip. The fact that at the tip the Mach number decreases so rapidly can be attributed to a rather large accumulation of secondary-flow low energy fluid as evidenced by low pressure ratio, mass flow, efficiency and high outflow angles near the blade tip. Near the hub of the rotor the inlet and discharge relative Mach numbers are essentially equal indicating practically no diffusion in the flow. At 90 and 100 percent of design speed, throttling has only a slight effect on the relative discharge Mach number. At 110 percent of design speed, the discharge Mach number is quite sensitive to throttling in a manner very similar to that observed in supersonic diffusers or compressors which is not surprising in view of the operating characteristic at this speed.

The radial distribution of absolute discharge Mach number M_2 is shown in figure 12. The negative slope from hub to tip is in accord with design requirements; however, except for the tip, the Mach number is considerably higher than design. At design speed, the Mach number is in excess of 0.9 for the major portion of the blade span.

The radial variation of total pressure ratio is shown in figure 13. Except for the tip and hub fall-off regions, the slope becomes steeper with increasing speed whereas the opposite is true at a given speed with increasing back pressure. At design speed, the total pressure ratio remains fairly constant with varying back pressure at $r_2 \approx 0.32$ foot because the relative discharge angle is axial. The hub half of the rotor produces a greater pressure ratio than design; the tip half, less. This is in accord with the fact that the discharge Mach numbers are greater than design indicating poorer diffusion than design. For those sections which turn beyond axial, the work input is increased as the static pressure is lowered and vice versa for sections which do not turn to axial. The sharp decrease in total pressure at the hub is undoubtedly caused by hub secondary flows which are aggravated by the radial inflows of blade surface boundary layer due to the fact that the fluid is turned considerably beyond axial.

The elemental weight-flow parameter as shown in figure 14 increases with radius at a rate equal to that predicted by design except for the region of rapidly decreasing values at the tip due to stall or secondary flow effects which effectively block the through-flow area.

Section efficiencies based on momentum change and temperature rise across the rotor are presented in figures 15 and 16, respectively. The rotor tip region is operating inefficiently with the severity of loss increasing with speed. Stalled condition of the rotor at 60 percent of design speed as stated previously and fall-off of total pressure ratio

at the higher speeds due to secondary flow effects and high Mach number level gave rise to the lower efficiencies at the tip region. No attempts were made to compute or estimate the magnitude of secondary flow effects. Mass-weighted values of the efficiencies presented in figure 9 show reasonable agreement for the two methods of computation although the radial distributions of the efficiencies are somewhat dissimilar.

Radial variation of the absolute flow angle leaving the rotor is presented in figure 17 for design speed only. The trend of the measured values agrees fairly well with that of design except at the tip region.

Blade-element performance.- The selection of blade sections to fulfill the requirements of the aerodynamic design of a given rotor is dependent upon valid two-dimensional cascade results. In the transonic regime, cascade data are questionable because of the difficulty of achieving an infinite cascade with a finite number of blades. However, cascade variables such as total-pressure loss coefficient, deviation angle and diffusion factor as functions of Mach number and incidence angle can be obtained from an analysis of rotor performance where blade-elemental characteristics are considered.

Accordingly, blade sections near the tip, mean, and hub regions were selected for blade-element study and the results are presented in figure 18. Care was exercised in choice of locations of the tip and hub elements so that they were not affected by low energy flow found near the boundaries.

The values obtained for an equivalent tip speed of 600 feet per second are not very meaningful for the reasons previously mentioned and, therefore, will not be discussed.

For the present investigation, the design angle of incidence was not obtained. The incidence angle for minimum loss for each blade-element at each operating condition was not always possible to determine because of the small range of incidence angle obtained by the rotor. However, from what evidence is available, the incidence angle for minimum loss appears to increase with tip speed at all elements. For instance, at the mean section selected, a value of about 5.5° at a tip speed of 900 feet per second was obtained as compared with a value of about 10.5° at the highest tip speed. Likewise, the minimum operating incidence angle obtainable increases with tip speed due primarily to the influence of the upstream wave pattern as described in the section entitled "Overall Performance."

Prediction of deviation angles by the use of a modified form of Carter's rule was found to yield values higher than those measured at the three stations. At optimum incidence angles, the flow was overturned about 1.0° at the tip section and about 4.0° at the hub section. These results tend to verify Carter's deviation angle rule in the transonic

region. The deviation angles are seen to decrease with incidence angle near the tip region while the opposite is true near the mean and hub regions. This trend cannot be explained although similar results have been reported in reference 2.

Measured values of diffusion factor are generally lower than that of design; however, at the tip section, the agreement was good since a measured value of 0.54 was obtained as compared to a design value of 0.57.

The required static pressure rise across the rotor was not obtained as indicated by the lower than design values of the diffusion coefficient, $\frac{\Delta p}{qF_c}$. The fact that, at the tip, the design value of diffusion was obtained, is indicative therefore of greater work input than predicted.

A comparison of the blade-element results with those obtained by a similar rotor reported in reference 2 is presented in the following table. The basis of comparison for the results of the two rotors is taken to be the inlet relative Mach number. In order to obtain similar Mach numbers, the results at a tip speed of 1,050 feet per second for the rotor of reference 2 are compared with the results at a tip speed of 900 feet per second for the present rotor.

	Design						Measured			
	Passage height, percent	r/r_t	ζ, deg	σ	ϕ, deg	t/c	M_{1R}	ω_{min}	η_{max}	$D\omega_{min}$
14-inch-diameter rotor (ref. 2); $\frac{U_t}{\sqrt{\theta}}$ = 1,050 ft/sec										
Tip	90.0	0.953	45.7	0.97	11.5	0.053	1.08	0.15	0.76	0.32
Mean	48.8	0.761	32.7	1.24	22.7	0.065	0.87	0.05	0.95	0.41
Hub	7.7	0.570	11.7	1.85	39.4	0.078	0.65	0.03	0.98	0.19
12-inch-diameter rotor (present); $\frac{U_t}{\sqrt{\theta}}$ = 900 ft/sec										
Tip	81.4	0.888	33.1	0.92	12.3	0.038	1.05	0.14	0.81	0.51
Mean	45.5	0.673	18.1	1.21	27.9	0.043	0.92	0.05	0.95	0.42
Hub	11.1	0.533	4.5	1.56	39.6	0.047	0.80	0.01	0.99	0.35

Both rotors have double-circular-arc sections and are similar with respect to blade shape and solidity. The major difference is the blade setting angle ζ which is from 7° to 14° greater and the thickness-chord ratio which is approximately 50 percent greater than the rotor of the present investigation.

As can be seen from the tabulated data, the Mach numbers at the tip and mean sections are essentially equal and at the hub where the largest divergence occurs, the Mach numbers are obviously below the "drag rise" level. The remarkable agreement of the measured losses of the two rotors indicates that for efficient operation the thickness-chord ratio and blade setting angle over the range presented are of secondary importance as compared with Mach number level.

As further evidence that such is the case, the minimum loss coefficient and diffusion factor at minimum loss of both rotors as a function of relative inlet Mach number are presented in figure 19. Although it was not possible to operate at the minimum loss conditions at lower tip speeds, the results for both rotors do overlap only at the tip section. It can be inferred that the critical Mach number for each section at which the loss begins to rise rapidly is independent of diffusion factor, blade-setting angle, and thickness-chord ratio within the range included by these tests. The usefulness of the diffusion factor becomes questionable at Mach numbers greater than 1.0 as can be seen in figure 20. At a tip speed of 900 feet per second, the minimum loss coefficient is in good agreement with the values presented in reference 7. At the higher speeds for roughly the same diffusion factors, the loss increases rapidly. The occurrence of shocks and the radical change in pressure distribution on an airfoil at transonic speeds would be expected to invalidate the assumptions inherent in the derivation of diffusion factor as a loading limit parameter.

SUMMARY OF RESULTS

A 12-inch-diameter transonic compressor rotor incorporating circular-arc sections was designed and tested in Freon-12 to investigate the operation of a rotor having a hub-tip radius ratio of 0.35 in the regime of near-sonic inlet axial velocity. The overall performance and blade-element characteristics at several speeds varying between 60 percent to 110 percent of design speed were determined. The following results, converted to air equivalent values, were obtained from this investigation:

(1) At a design equivalent tip speed of 1,000 feet per second, a specific weight flow of air of 42.0 $lb/sec/ft^2$ was obtained with a mass-weighted pressure ratio of 1.38 at a peak efficiency of 80 percent. A maximum specific weight flow of 42.13 $lb/sec/ft^2$ was reached at 110 percent of design speed with an efficiency of 75 percent and a mass-weighted pressure ratio of 1.45. The maximum efficiency of 85 percent was attained at 60 and 90 percent of design speed.

(2) The design weight flow of 43.2 lb/sec/ft^2 was not obtained because of the supersonic wave pattern generated by the curved "entrance region" on the convex surface of the blades which restricted the axial Mach number to a value of 0.81. Because of the supersonic nature of flow, the minimum angle of incidence for this rotor is determined by the blade surface angles and not by back pressure or the occurrence of choking flow in the blades.

(3) The performance of the outer third of the blade span was extremely poor, principally because of the higher inlet Mach number rather than blade loading. Measured losses were considerably greater than expected based upon design diffusion factor and the correlation presented in NACA Research Memorandum E53D01.

(4) Comparison of results with those of a rotor similar in camber and solidity (NACA Research Memorandum E54I29) indicates that for efficient operation the thickness-chord ratio and blade setting angle over the range presented are of secondary importance as compared with relative inlet Mach number level.

Langley Aeronautical Laboratory,
National Advisory Committee for Aeronautics,
Langley Field, Va., May 23, 1956.

REFERENCES

1. Savage, Melvyn, and Felix, A. Richard: Investigation of a High-Performance Axial-Flow Compressor Transonic Inlet Rotor Designed for 37.5 Pounds Per Second Per Square Foot of Frontal Area - Aerodynamic Design and Overall Performance. NACA RM L55A05, 1955.

2. Montgomery, John C., and Glaser, Frederick W.: Experimental Investigation of a 0.4 Hub-Tip Diameter Ratio Axial-Flow Compressor Inlet Stage at Transonic Inlet Relative Mach Numbers. II - Stage and Blade-Element Performance. NACA RM E54I29, 1955.

3. Lewis, George W., Jr., and Schwenk, Francis C.: Experimental Investigation of a Transonic Axial-Flow-Compressor Rotor With Double-Circular-Arc Airfoil Blade Sections. II - Blade-Element Performance. NACA RM E54J08, 1955.

4. Robbins, William H., and Glaser, Frederick W.: Investigation of an Axial-Flow-Compressor Rotor With Circular-Arc Blades Operating Up to a Rotor-Inlet Relative Mach Number of 1.22. NACA RM E53D24, 1953.

5. Ferri, Antonio: Three Dimensional Effects in Supersonic Compressors. Part I - Introductory Remarks on the Design Problem of Supersonic Compressors. PIBAL Rep. No. 233 (Contract No. Nonr-741(00)), Oct. 1953.

6. Savage, Melvyn, and Beatty, Loren A.: A Technique Applicable to the Aerodynamic Design of Inducer-Type Multistage Axial-Flow Compressors. NACA TN 2598, Mar. 1952.

7. Lieblein, Seymour, Schwenk, Francis C., and Broderick, Robert L.: Diffusion Factor for Estimating Losses and Limiting Blade Loadings in Axial-Flow-Compressor Blade Elements. NACA RM E53D01, 1953.

8. Goldberg, Theodore J.: Experimental Investigation of an Axial-Flow Supersonic Compressor Having Sharp Leading-Edge Blades With an 8-Percent Mean Thickness-Chord Ratio. NACA RM L54K16, 1954.

9. Carter, A. D. S.: The Low Speed Performance of Related Aerofoils in Cascade. National Gas Turbine Establishment Rep. No. R.55, British Ministry of Supply, Sept. 1949.

10. Andrews, S. J.: Tests Related to the Effect of Profile Shape and Camber-Line on Compressor Cascade Performance. R. & M. No. 2743, British A.R.C., Oct. 1949.

11. Boxer, Emanuel, and Erwin, John R.: Investigation of a Shrouded and an Unshrouded Axial-Flow Supersonic Compressor. NACA RM L50G05, 1950.

12. Kantrowitz, Arthur: The Supersonic Axial-Flow Compressor. NACA Rep. 974, 1950. (Supersedes NACA ACR L6D02.)

13. Boxer, Emanuel, Sterrett, James R., and Wlodarski, John: Application of Supersonic Vortex-Flow Theory to the Design of Supersonic Impulse Compressor- or Turbine-Blade Sections. NACA RM L52B06, 1952.

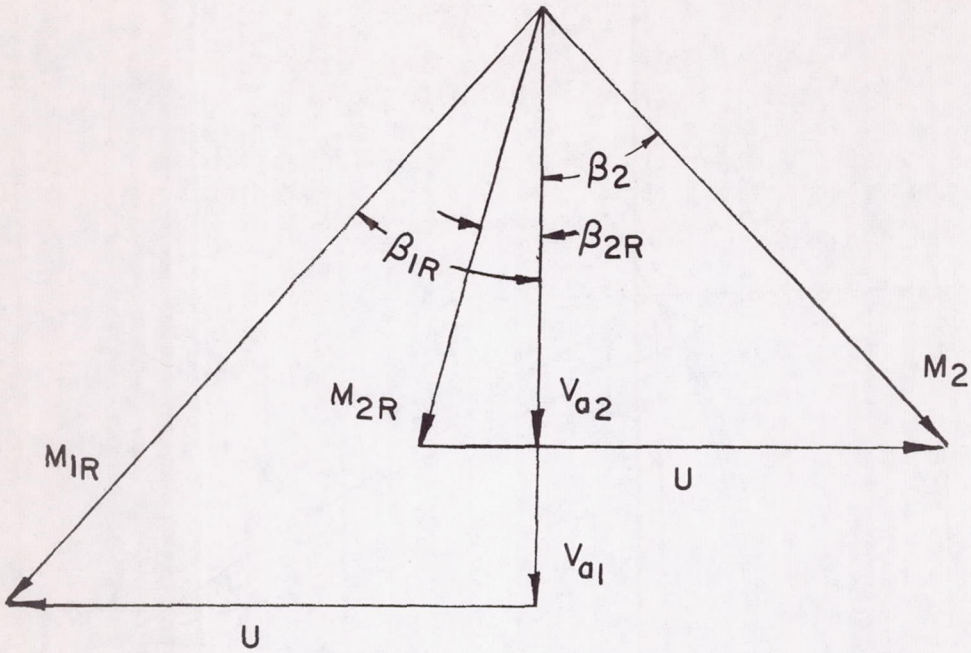

$\frac{r_1}{r_t}$	$\frac{r_2}{r_t}$	M_{1R}	β_{1R}, deg	M_{2R}	β_{2R}, deg	M_2	β_2, deg	$\frac{V_{a2}}{V_{a1}}$	D	$\frac{\Delta p}{qF_c}$	$\frac{P_2}{P_1}$
[a]1.000	1.000	1.40	44.4	0.84	39.8	0.73	29.2	0.71	0.51	0.43	1.46
.883	.888	1.31	41.1	.75	30.7	.76	32.5	.70	.57	.49	1.46
[a].800	.800	1.26	38.1	.70	23.5	.77	34.5	.70	.59	.51	1.45
.655	.673	1.19	33.0	.65	8.0	.82	37.8	.70	.59	.54	1.42
[a].600	.600	1.16	30.5	.64	1.5	.83	39.0	.69	.59	.52	1.39
.502	.533	1.12	26.3	.67	-9.8	.88	40.8	.71	.54	.50	1.37
[a].400	.400	1.07	21.4	.75	-20.0	.95	42.0	.71	.45	.36	1.31

[a]Design station.

Figure 1.- Velocity diagram design data using air values.

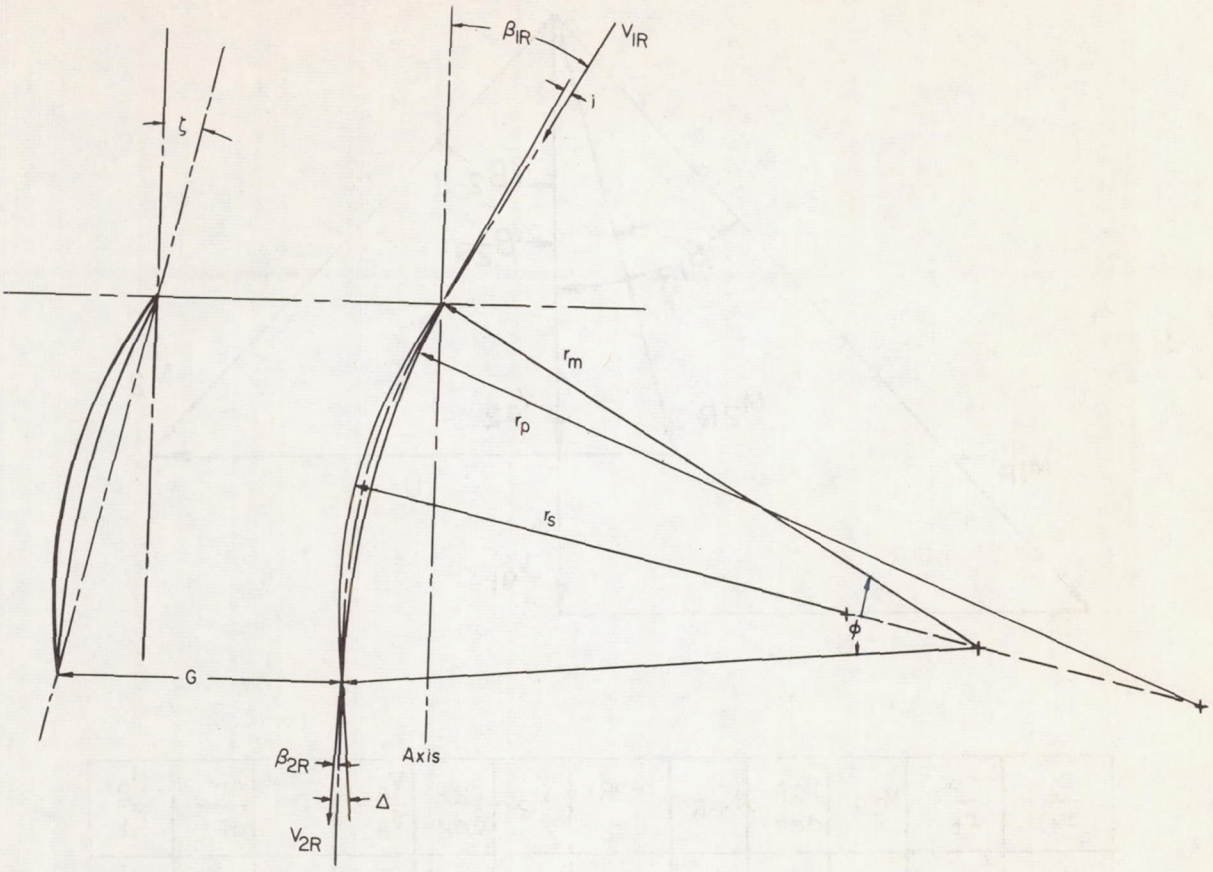

$\frac{r}{r_t}$	φ, deg	i, deg	Δ, deg	σ	t/c	r_{le}, in.	r_s, in.	r_p, in.	r_m, in.
1.000	5.3	2.0	2.9	0.8	0.035	0.0010	10.82	52.49	27.58
.800	16.9	2.0	4.0	1.0	.040	.0025	5.69	17.55	8.49
.600	34.2	2.0	6.9	1.33	.045	.0050	3.40	5.81	4.25
.400	50.4	2.0	8.0	2.0	.050	.0075	2.51	3.60	2.94

Figure 2.- Rotor blade element details.

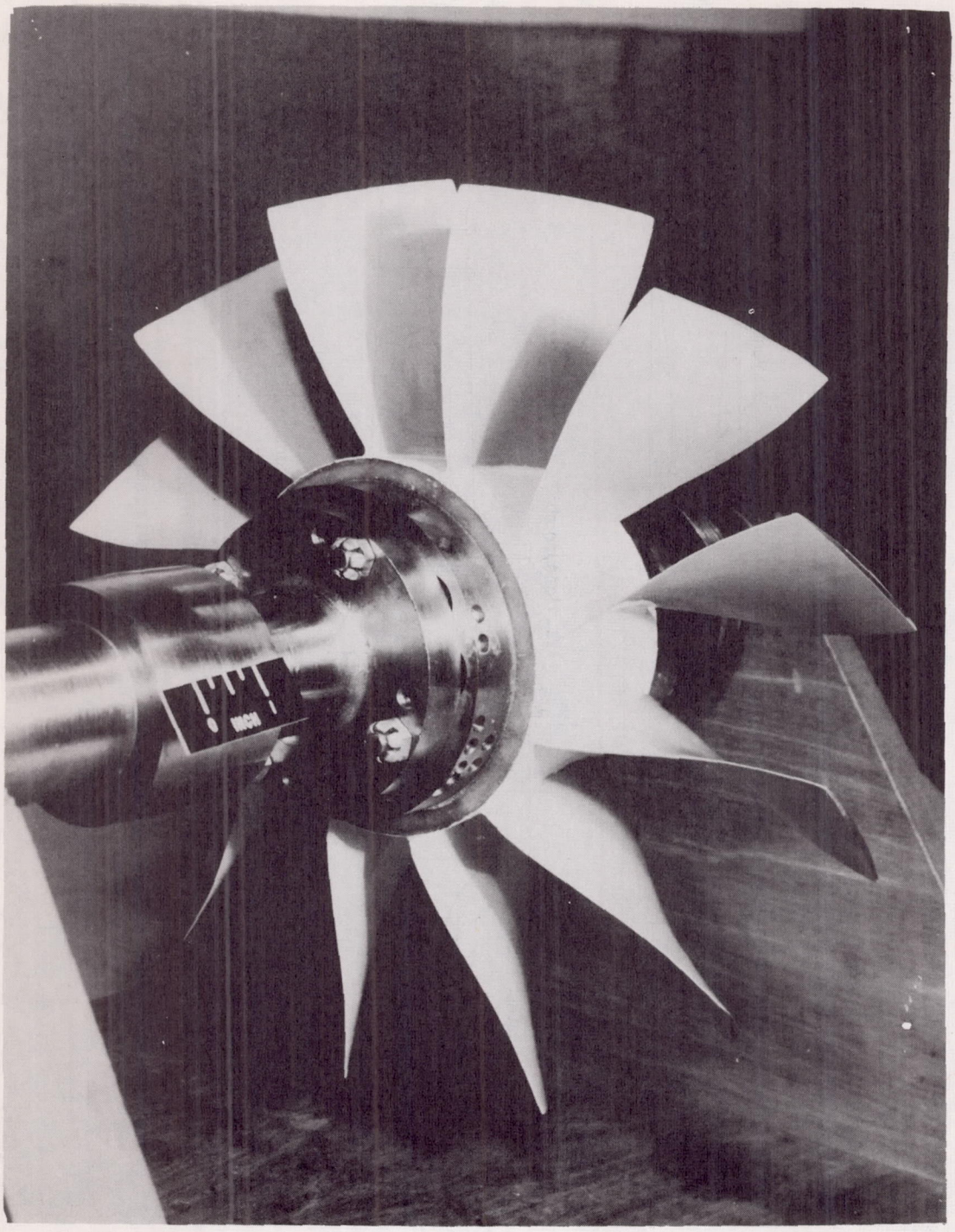

Figure 3.- Three-quarter rear view of test rotor. L-88038

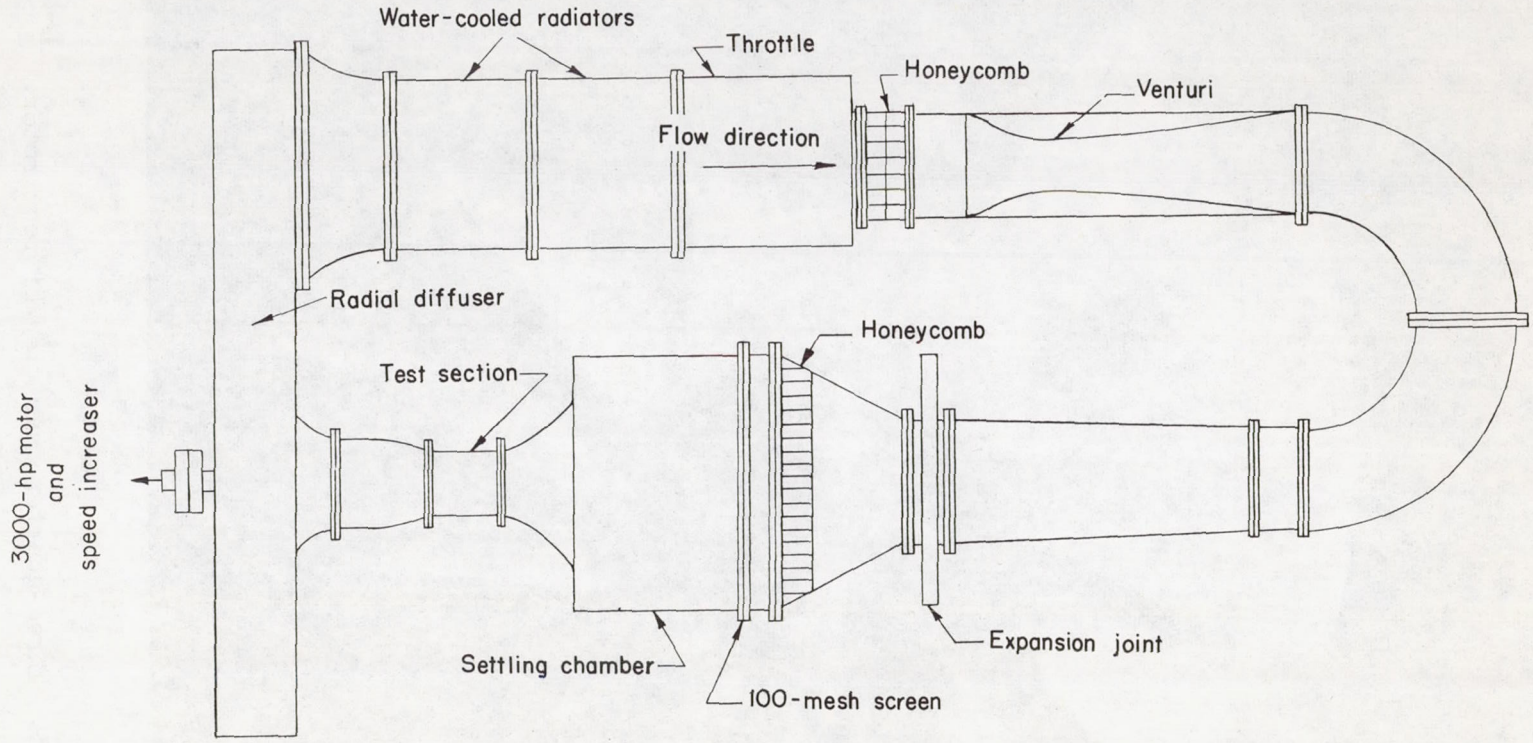

Figure 4.- Schematic diagram of compressor test stand.

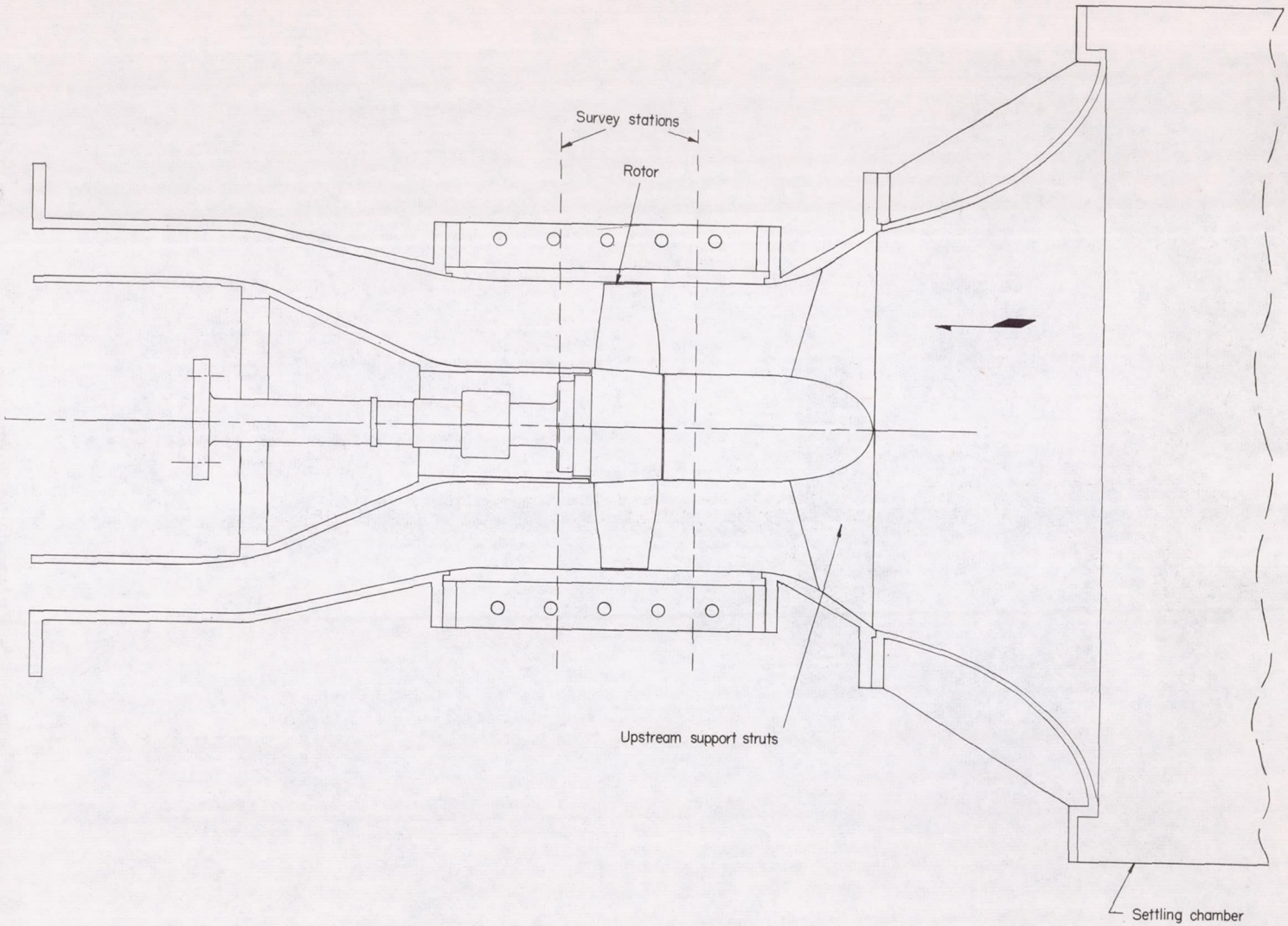

Figure 5.- Test section detail.

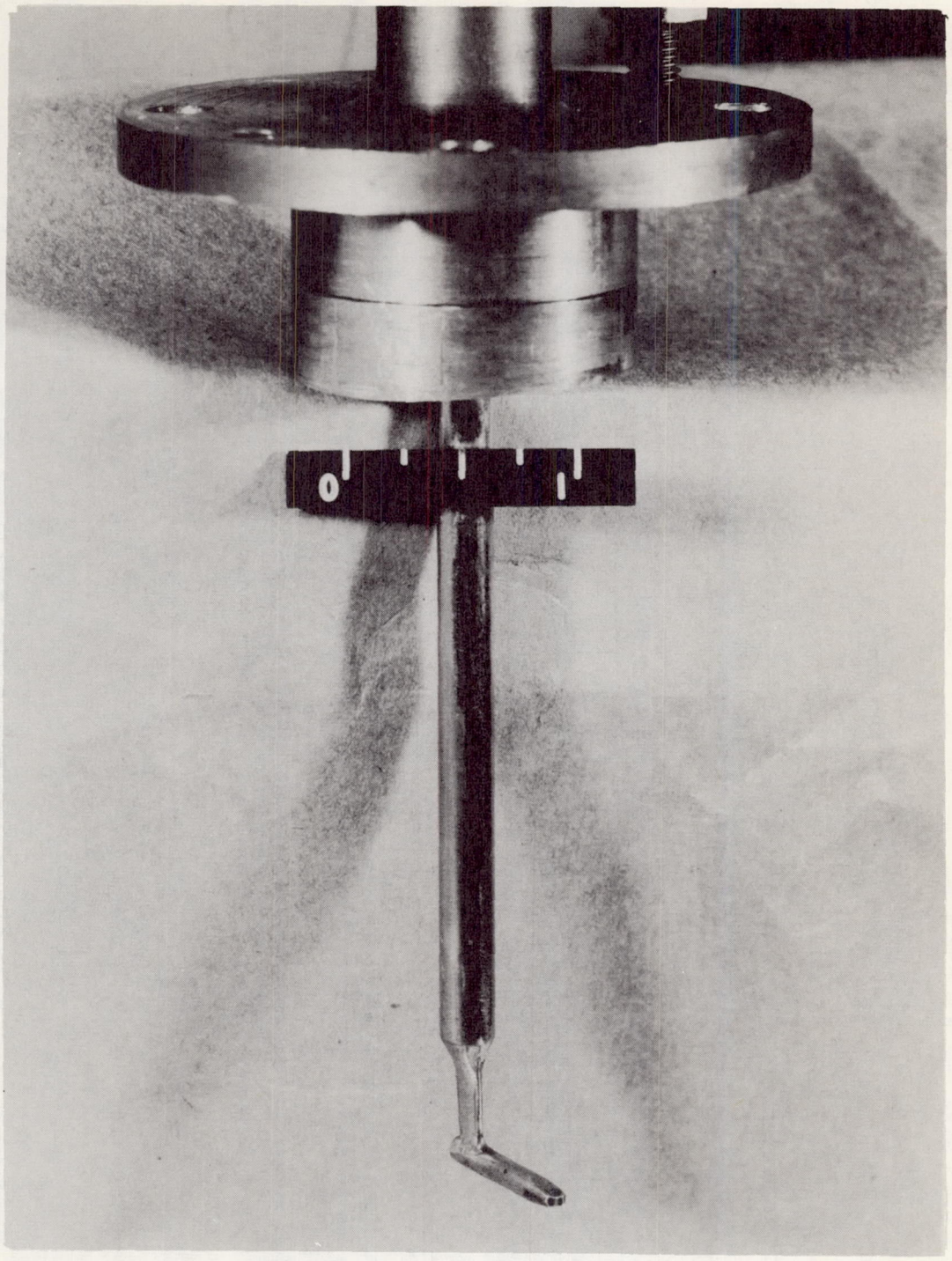

Figure 6.- Prism-type survey probe. L-85988

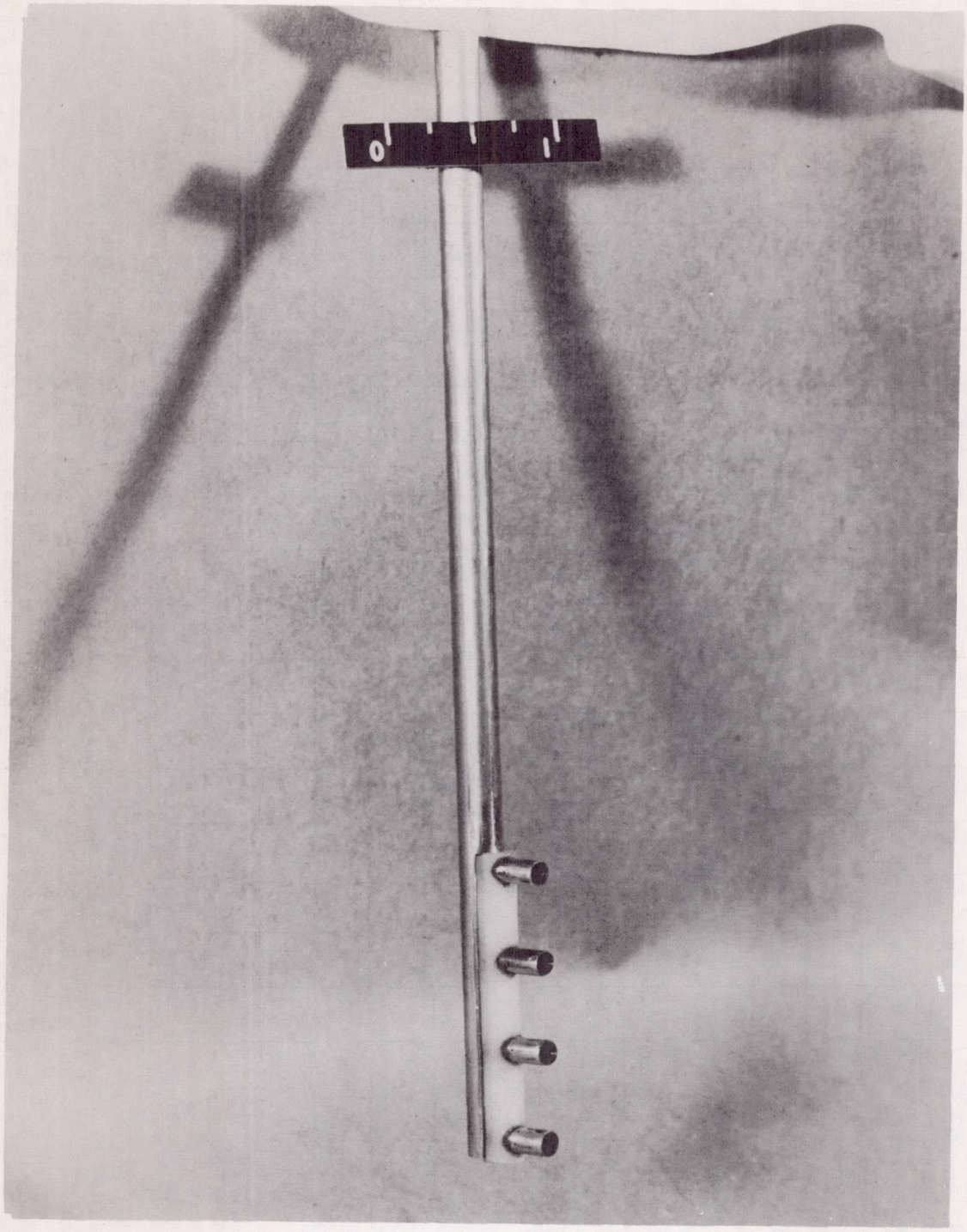

Figure 7.- Four-bell stagnation-temperature rake. L-85987

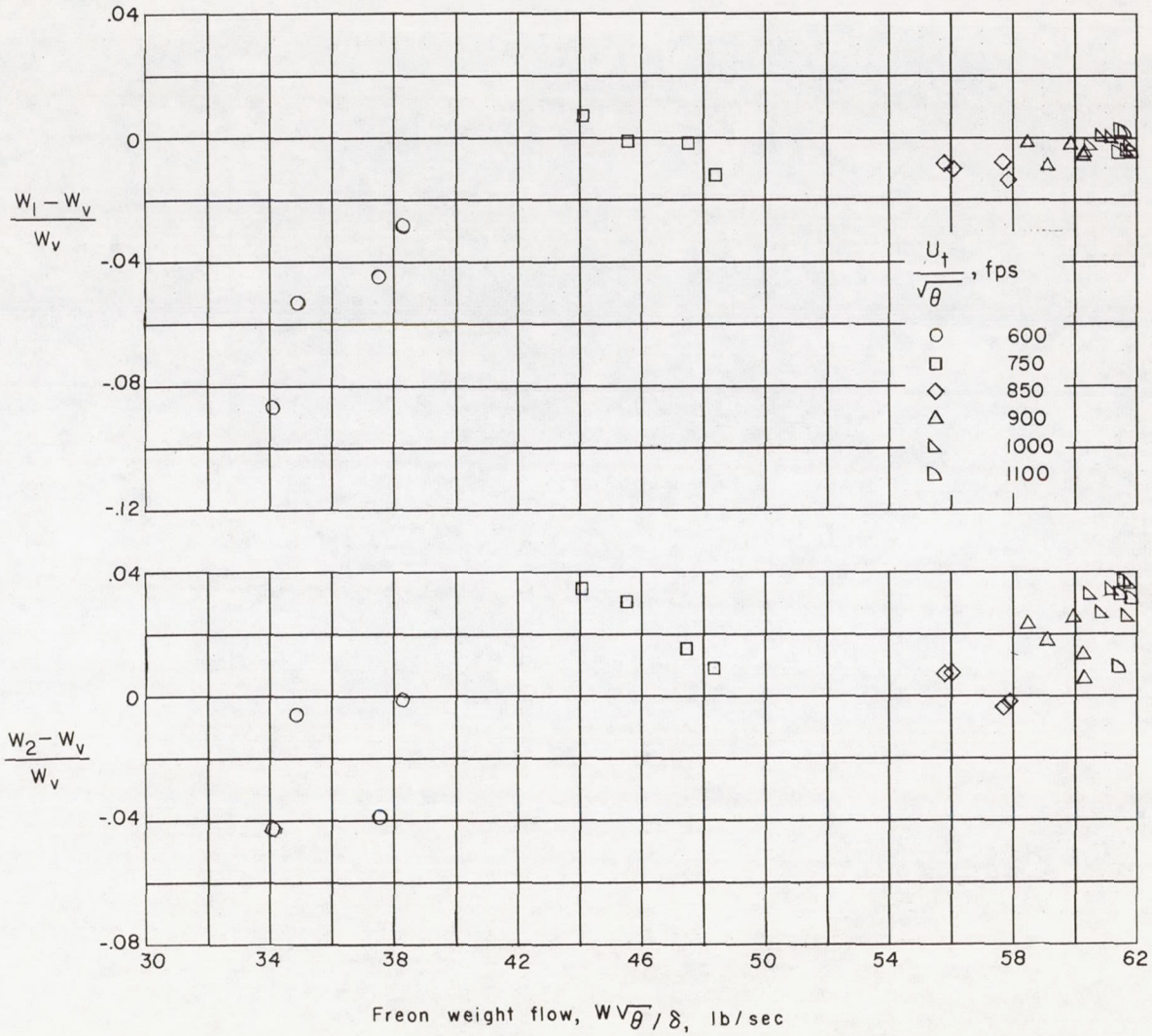

Figure 8.- Comparison of weight-flow measurements at various tip speeds.

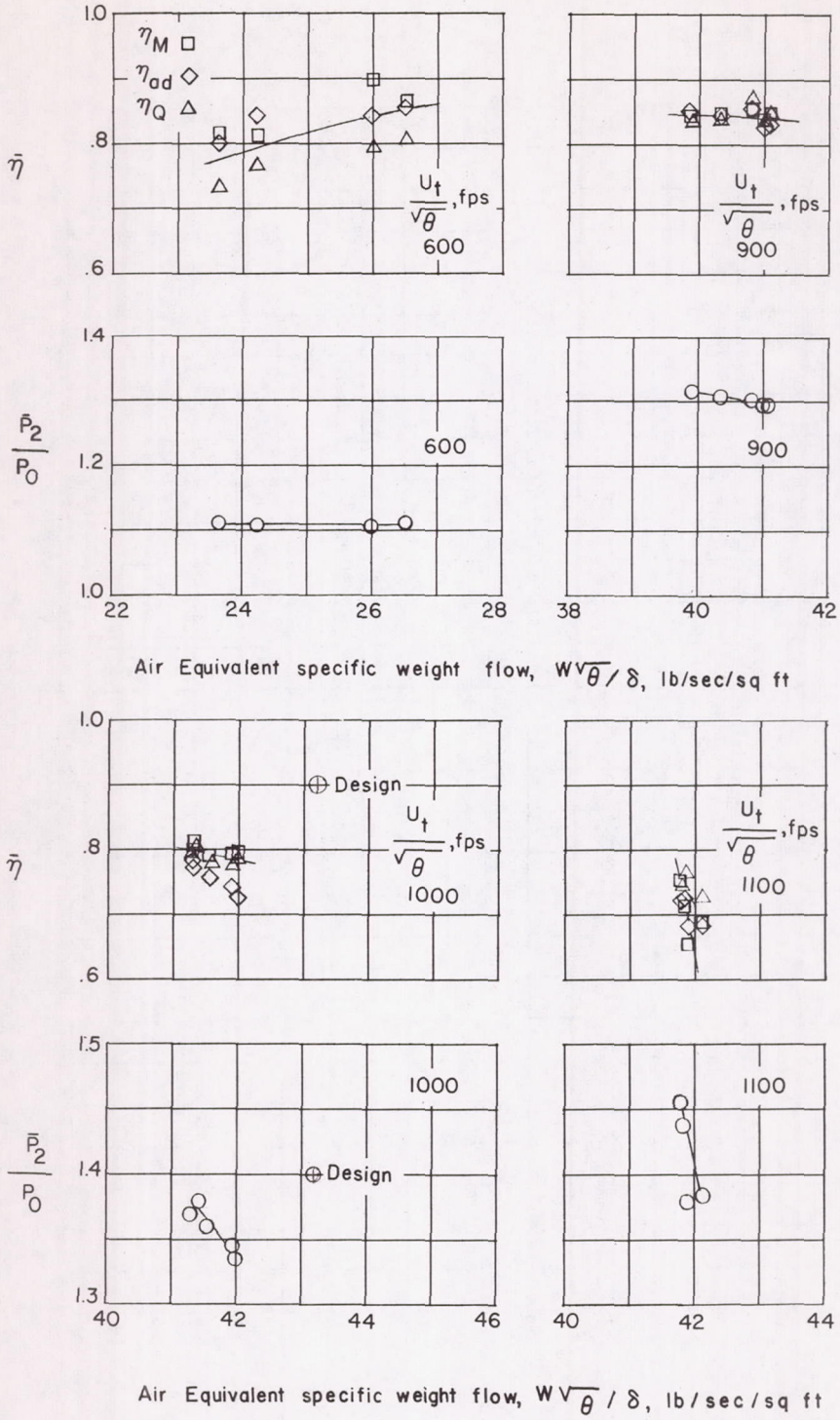

Figure 9.- Overall rotor performance.

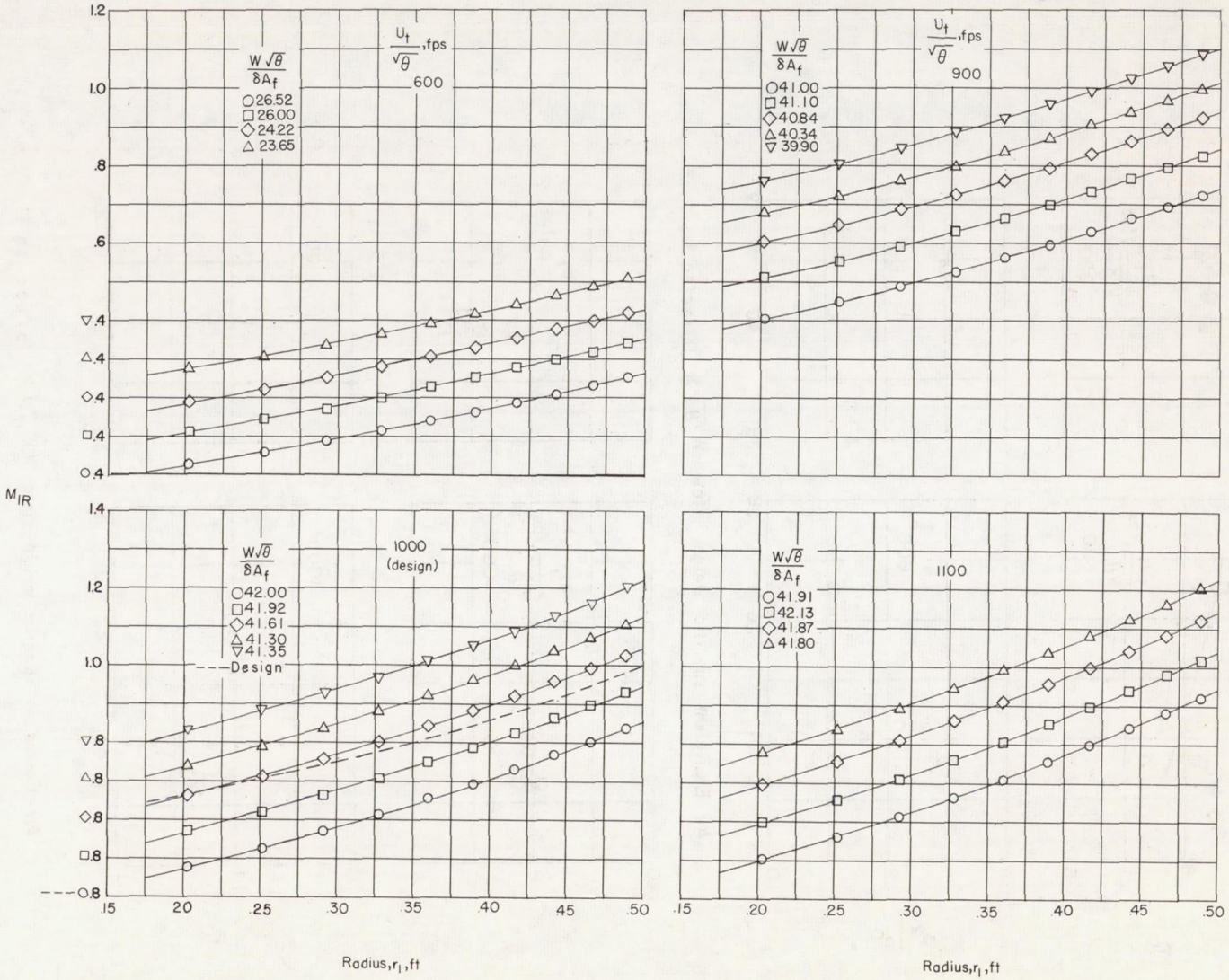

Figure 10.- Radial variation of inlet relative Mach number.

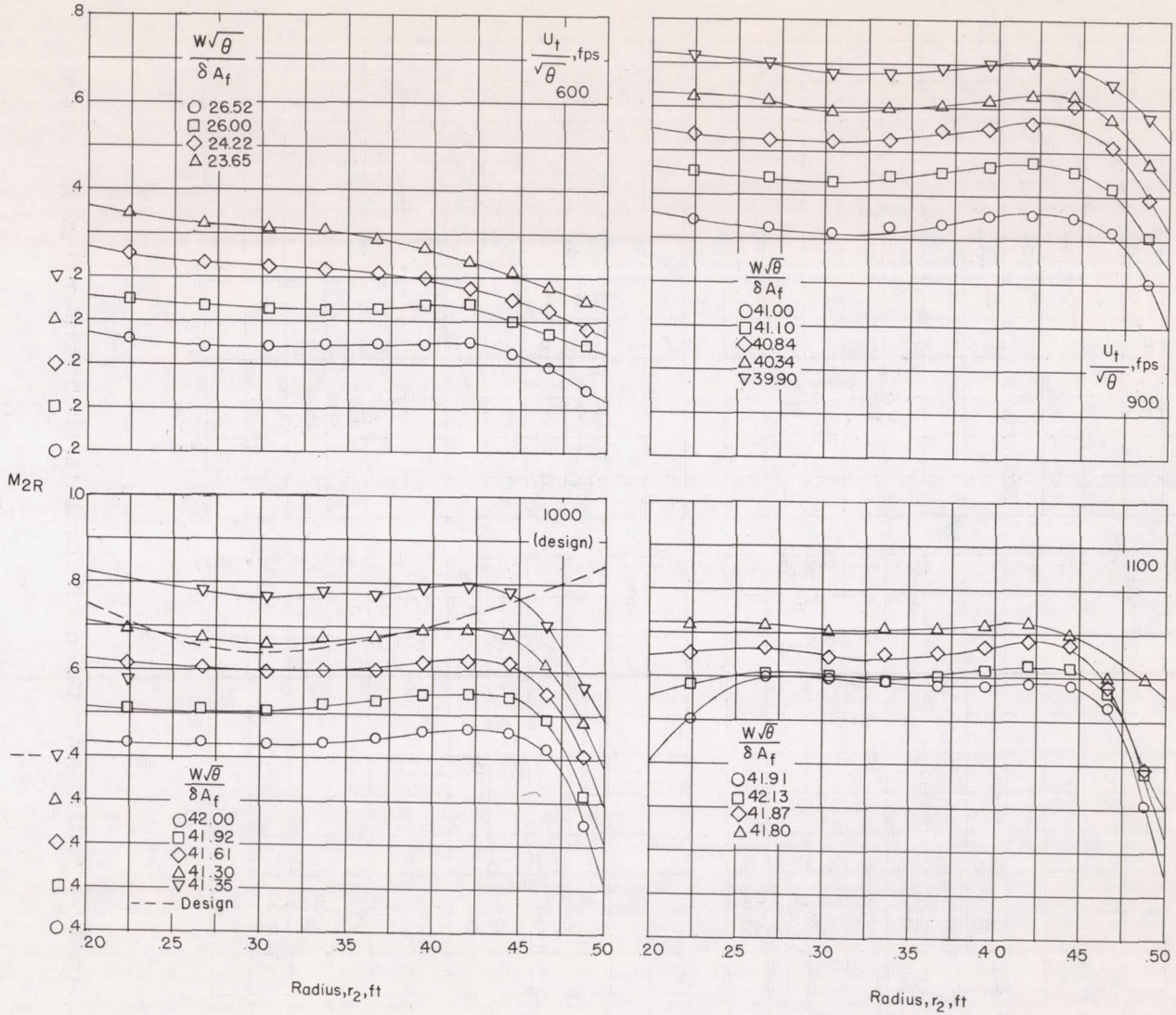

Figure 11.- Radial variation of relative Mach number leaving rotor.

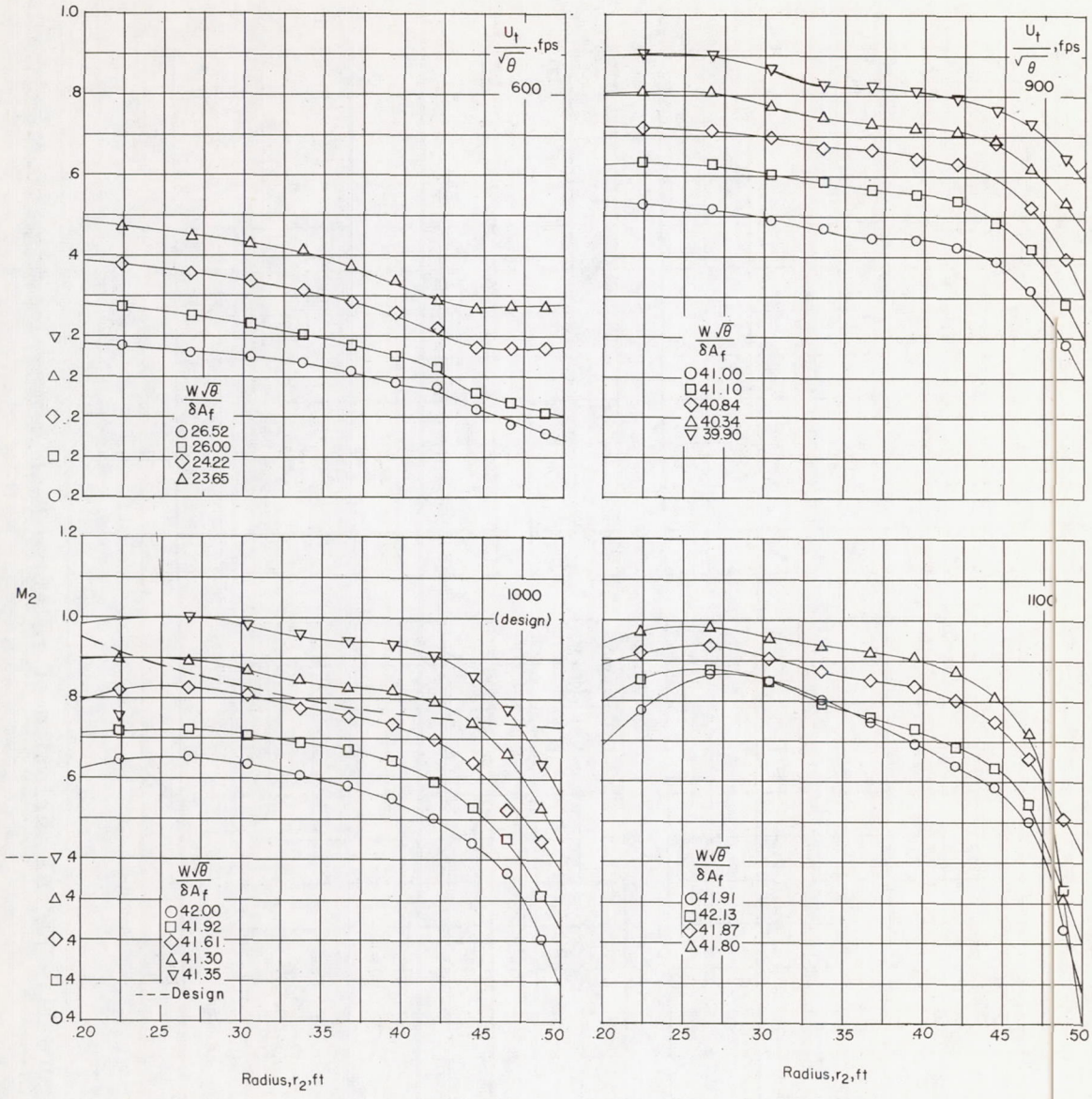

Figure 12.- Radial variation of absolute Mach number leaving rotor.

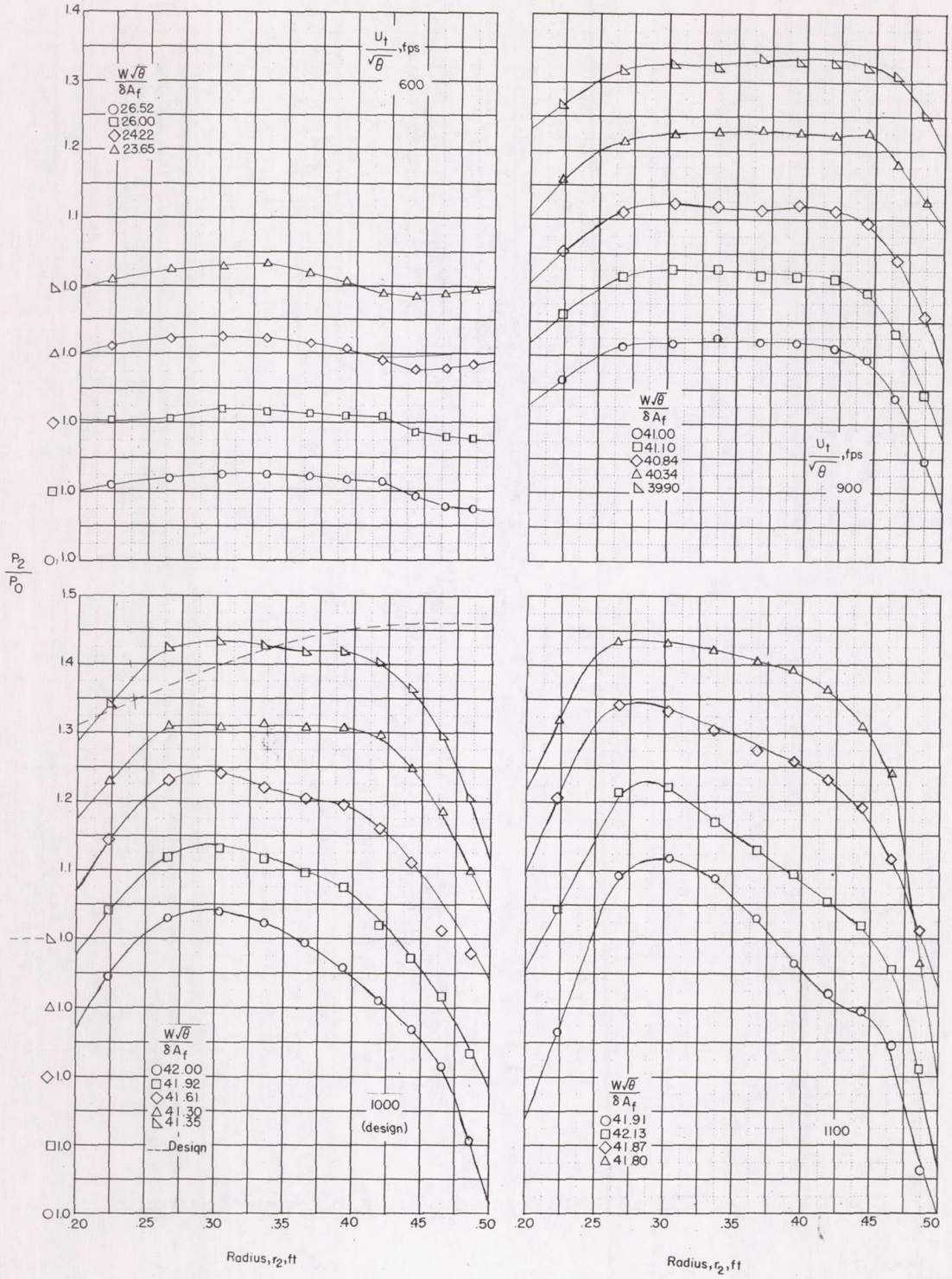

Figure 13.- Radial variation of total pressure ratio.

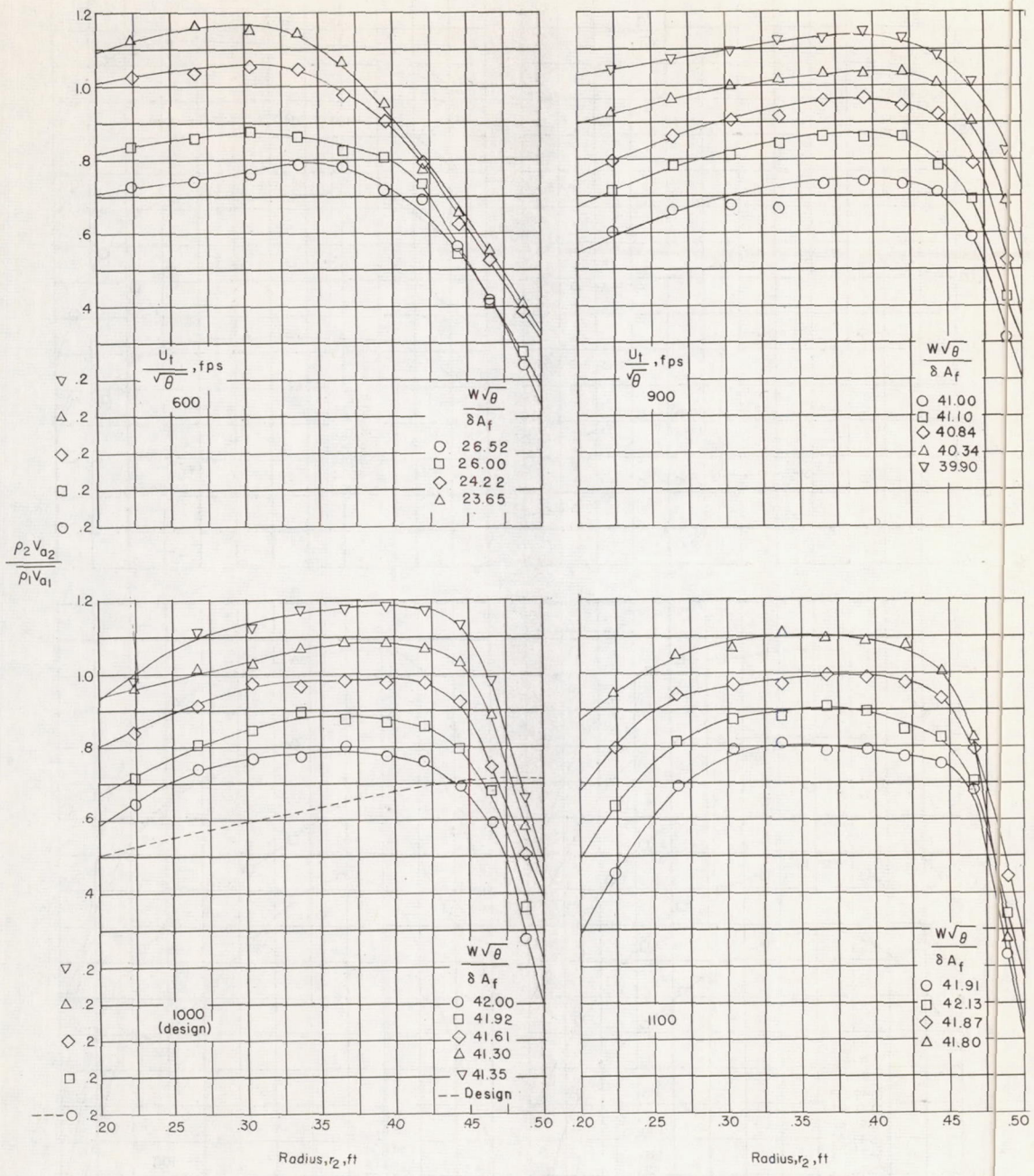

Figure 14.- Radial variation of weight-flow parameter.

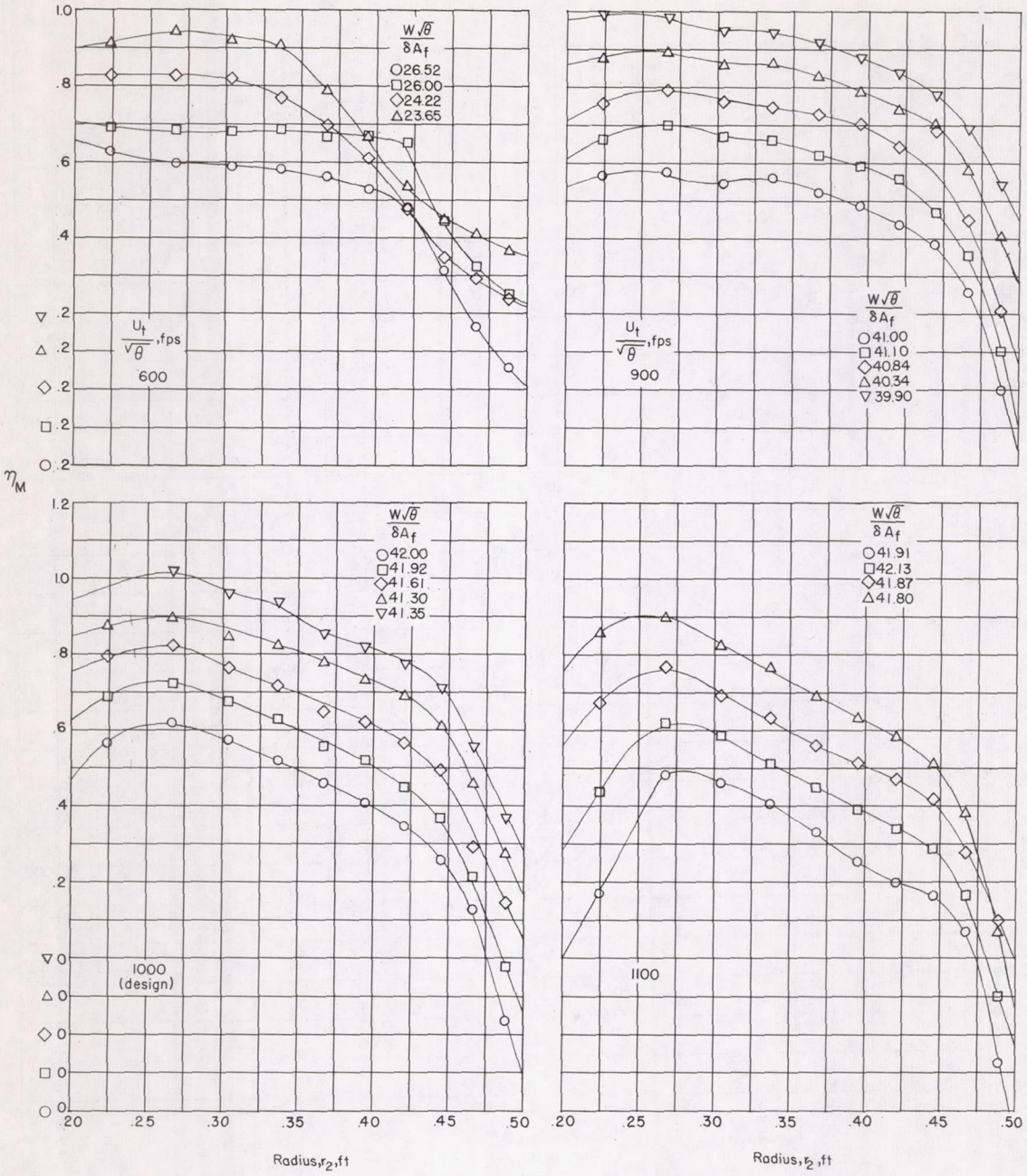

Figure 15.- Radial variation of adiabatic efficiency based on momentum change.

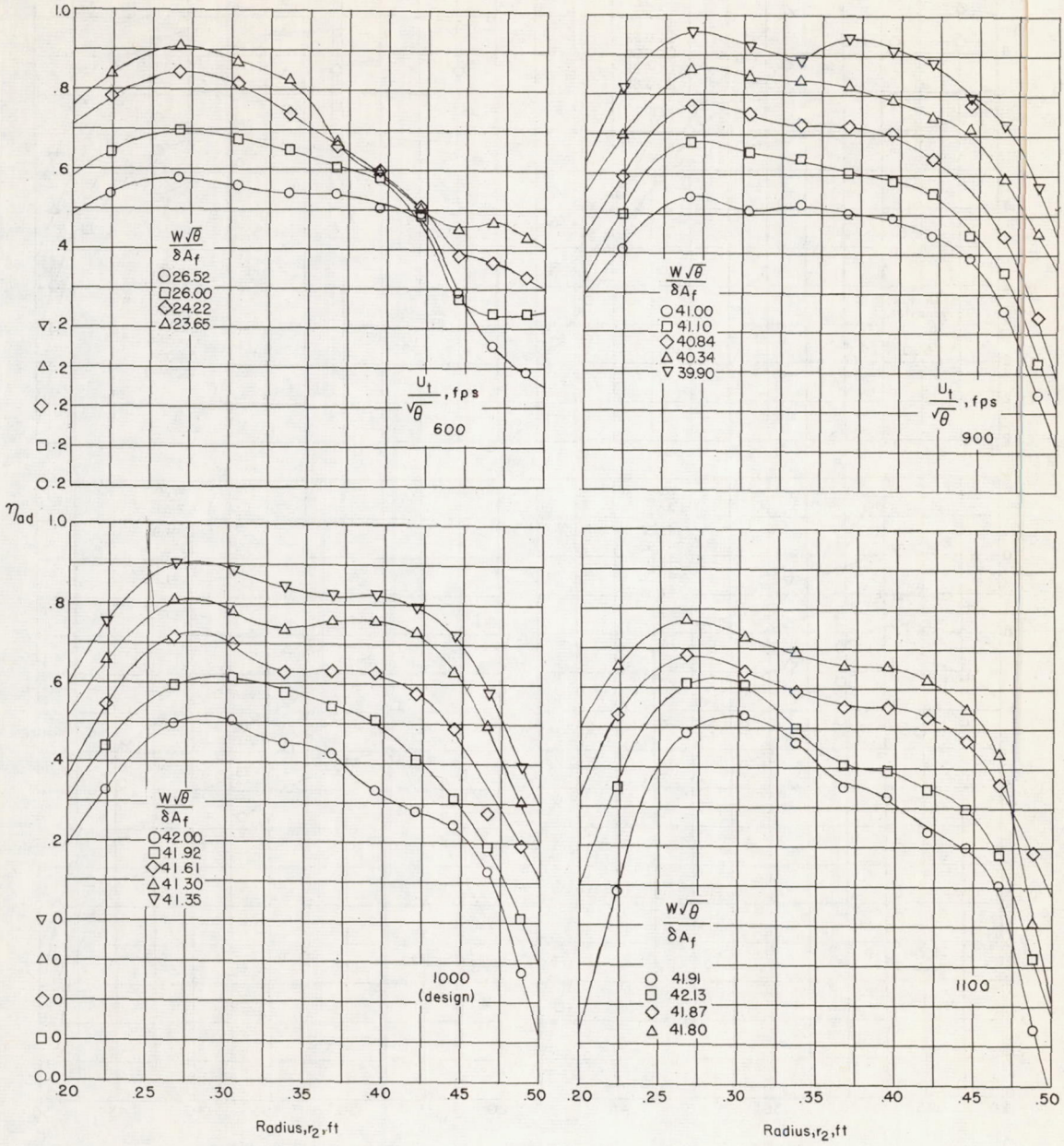

Figure 16.- Radial variation of adiabatic efficiency based on temperature measurements.

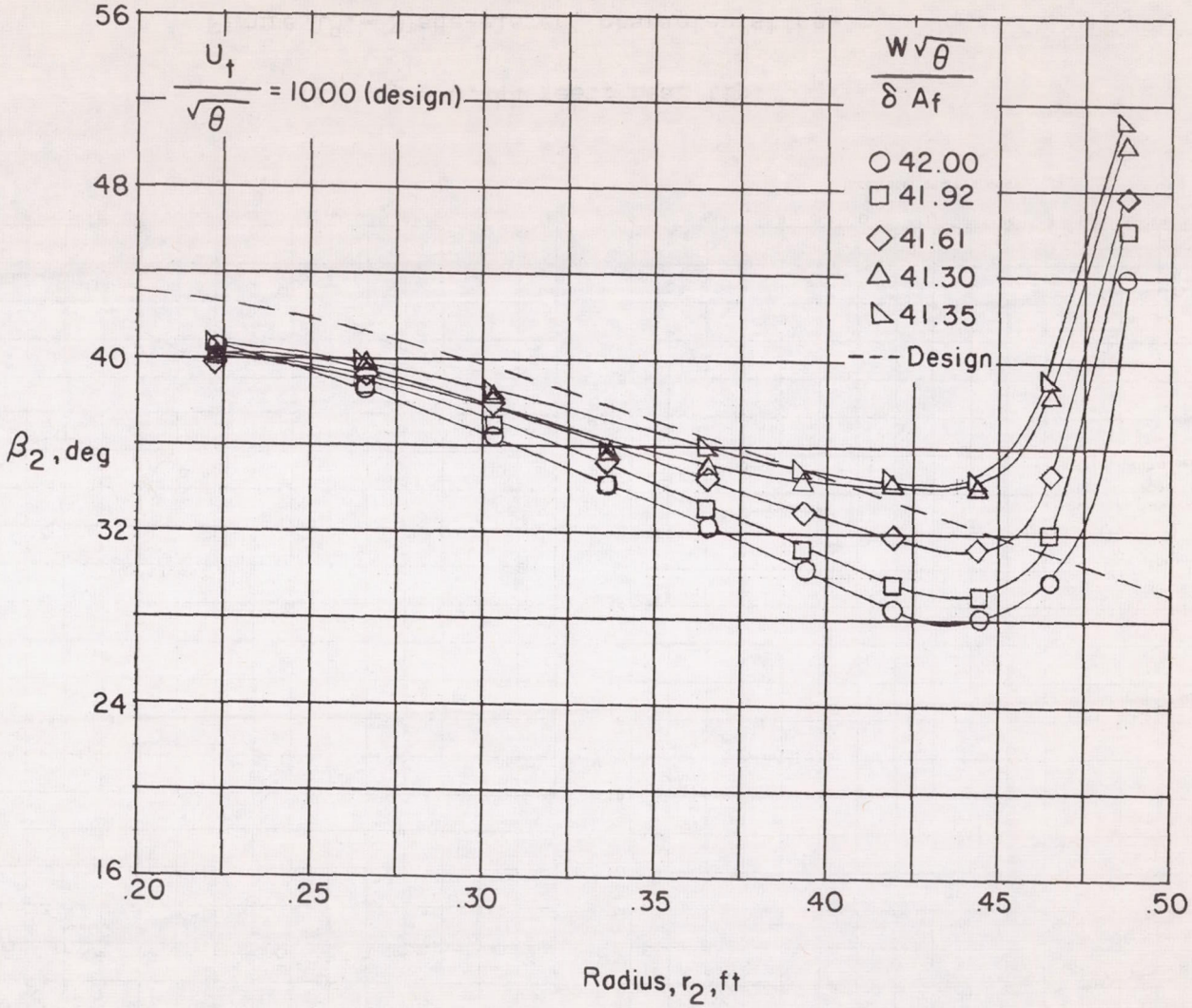

Figure 17.- Radial variation of absolute flow angle leaving rotor at design speed.

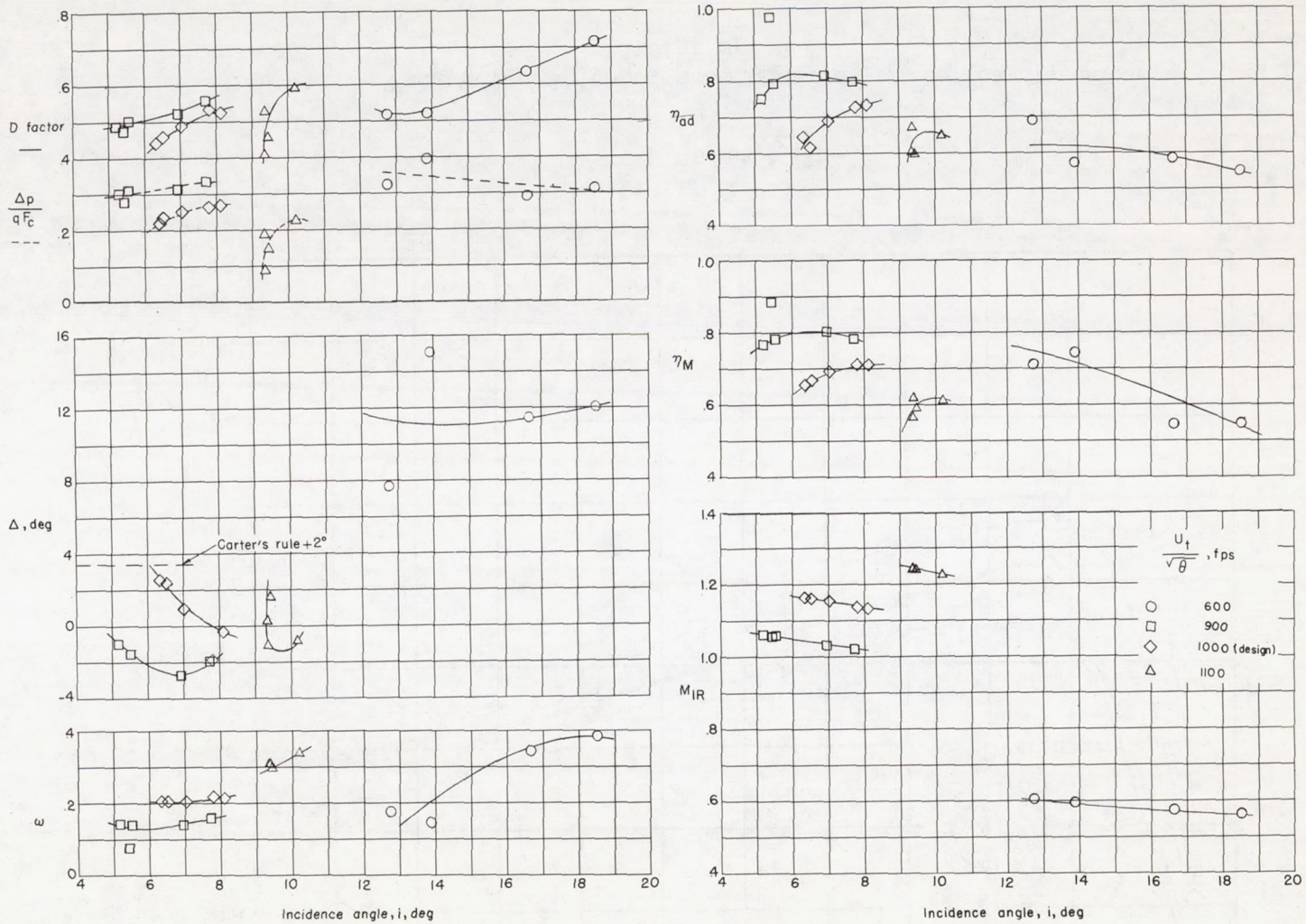

(a) r_2 = 0.444 feet; near tip.

Figure 18.- Blade-element characteristics.

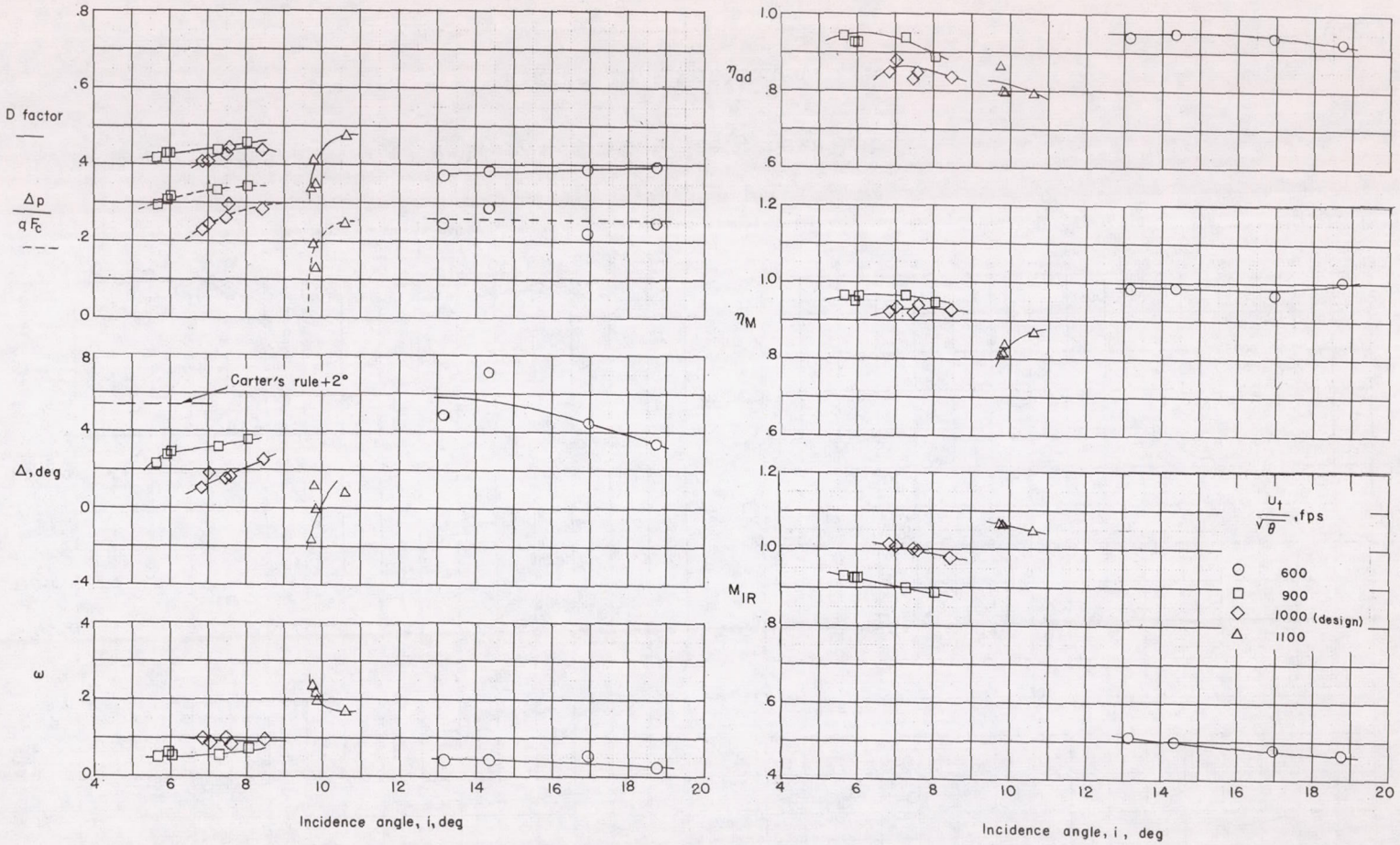

(b) r_2 = 0.3365 feet; near mean.

Figure 18.- Continued.

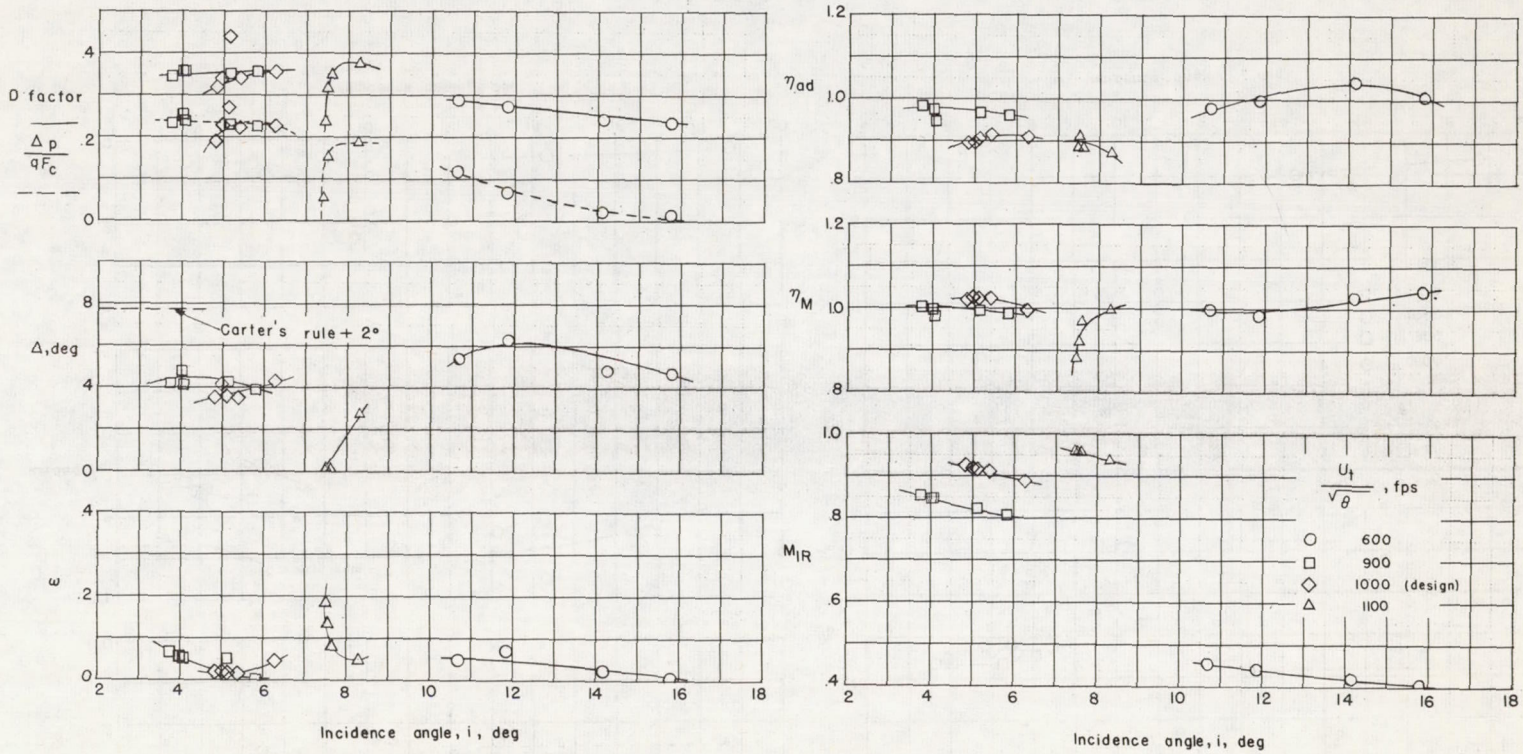

(c) r_2 = 0.2665 feet; near hub.

Figure 18.- Concluded.

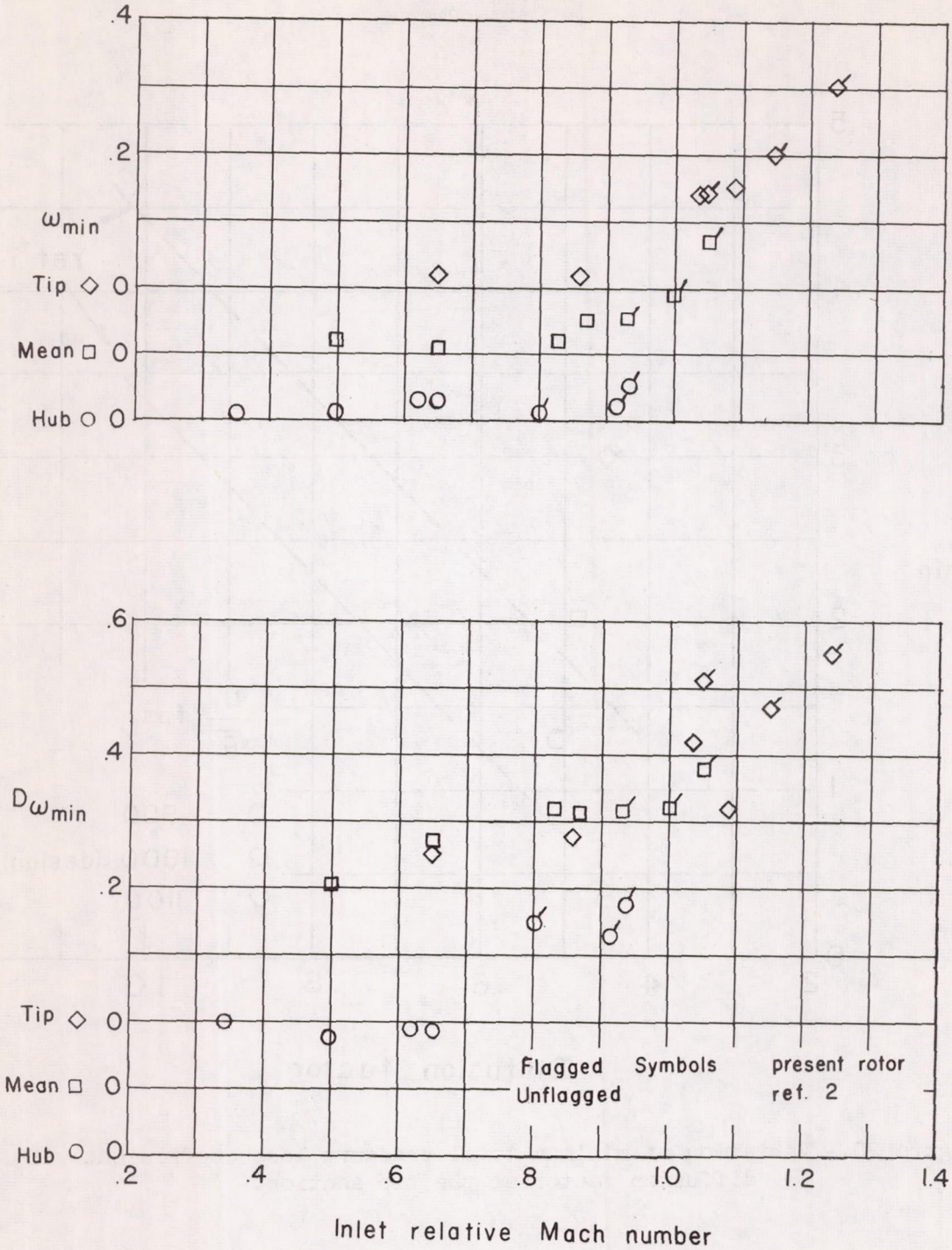

Figure 19.- Variation of minimum loss coefficient and diffusion factor with inlet relative Mach number for two rotors.

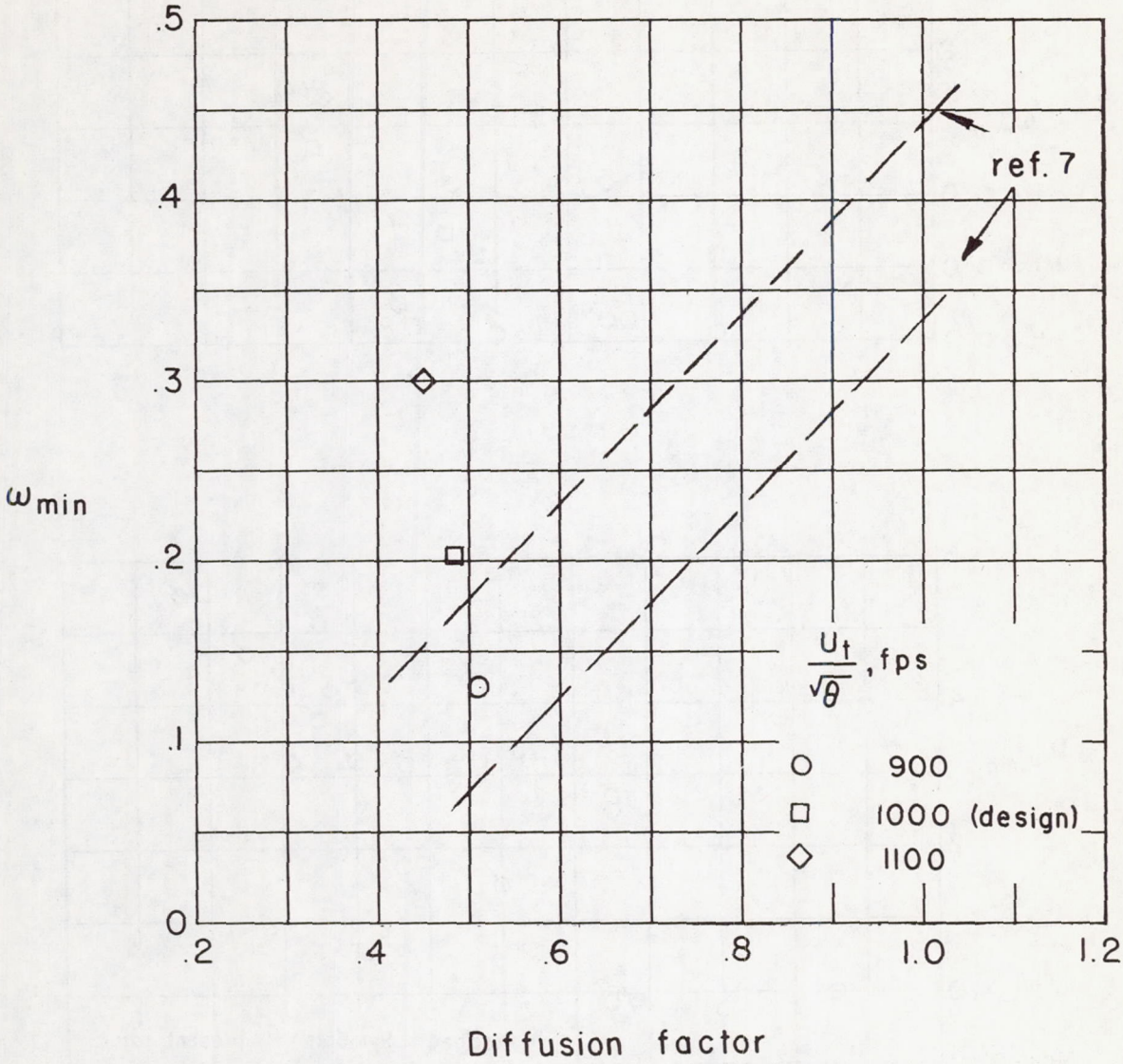

Figure 20.- Variation of minimum total pressure loss coefficient with diffusion factor at the tip section.

NACA - Langley Field, Va.